Modulation of cannabinoid receptor 2 alters neuroinflammation and reduces formation of alpha-synuclein aggregates in a rat model of nigral synucleinopathy

Valerie Joers[1,2,3*], Benjamin C Murray[4], Caroline McLaughlin[4], Danielle Oliver[4], Hannah Staley[1,2,3], Jazmyn Coronado[1,2,3], Cindy Achat-Mendes[5], Sanam Golshani[4], Sean D. Kelly[4], Matthew Goodson[4], Danica Lee[4], Fredric P. Manfredsson[6], Bob M. Moore[7], Malú Gámez Tansey[1,2,3,8]

[1] Department of Neuroscience, University of Florida College of Medicine, Gainesville, Florida
[2]Center for Translational Research in Neurodegenerative Disease, University of Florida College of Medicine, Gainesville, Florida
[3]McKnight Brain Institute, University of Florida, Gainesville, Florida
[4]Department of Physiology, Emory University, Atlanta, Georgia
[5]Department of Biology, Georgia Gwinnett College, Lawrenceville, Georgia
[6]Parkinson's Disease Research Unit, Department of Translational Neuroscience, Barrow Neurological Institute, Phoenix, Arizona
[7]Department of Pharmaceutical Sciences, University of Tennessee Health Science Center, Memphis, Tennessee
[8]Norman Fixel Institute for Neurological Diseases, University of Florida Health, Gainseville, Florida

*Corresponding author

ABSTRACT
There is growing evidence that neuroinflammation accompanies and may promote progression of alpha-synuclein (Asyn)-induced nigral dopaminergic (DA) degeneration. Research into the disequilibrium of microglial phenotypes has become an area of intense focus in neurodegenerative disease as a potential mechanism that contributes to chronic neuroinflammation and neuronal loss in Parkinson's disease (PD). From a therapeutic perspective, development of immunomodulatory strategies that dampen overproduction of pro-inflammatory cytokines from chronically activated immune cells and induce a pro-phagocytic phenotype is expected to promote Asyn removal and protect vulnerable neurons. Cannabinoid receptor-2 (CB2) is highly expressed on activated microglia and peripheral immune cells, is upregulated in the substantia nigra of PD patients and in mice models of nigral degeneration. Furthermore, modulation of CB2 protects against rotenone-induced nigral degeneration, however CB2 has not been pharmacologically and selectively targeted in an alpha-synuclein focused model of PD. We find that 7 weeks of peripheral SMM-189 treatment reduced phosphorylated (pSer129) alpha-synuclein in the substantia nigra compared to vehicle treatment. Additionally, SMM-189 altered brain immune cell phenotypes with increased CD68 and decreased CD163 protein expression, elevated wound healing immune mediator gene expression and modified leukocyte infiltration kinetics as determined by flow cytometry. Additionally, peripheral immune cells increased wound healing non-classical monocytes and decreased pro-inflammatory classical monocytes. Together, results suggest that targeting CB2 with SMM-189 biased immune cell function toward a phagocytic phenotype and reduced toxic species of alpha-synuclein aggregation. This study highlights that CB2 may be a target for proteinopathies with notable accompanying inflammation.

Keywords: Parkinson's disease, cannabinoid receptor 2, alpha-synuclein, microglia phenotype

Background

Research into the disequilibrium of microglial phenotypes has become an area of intense focus in neurodegenerative disease as a potential mechanism that contributes to disease pathophysiology, including chronic neuroinflammation and neuronal loss (1, 2). More specifically, microglia dynamically transition from homeostatic to disease-associated phenotypes that has varying transcriptional and functional profiles. In Parkinson's disease (PD), activated microglia have been described in postmortem brain analysis while single-cell transcriptomic studies have identified disease-specific increases in midbrain microglia with two of the three main microglia clusters involved in the inflammatory response (3). Findings from animal models demonstrate that overexpression or fibrillar alpha-synuclein (Asyn) in the brain influences microglial phenotypes and infiltration of peripheral immune cells (4-6). From a therapeutic perspective, the development of immunomodulatory strategies that dampen overproduction of pro-inflammatory cytokines from chronically activated immune cells and promote a pro-phagocytic phenotype is expected to protect vulnerable neurons and promote toxic Asyn removal.

Cannabinoid receptor 2 (CB2) is highly expressed on activated microglia and peripheral immune cells including circulating monocytes (7). Due to its abundant presence on immune cells, CB2 has emerged as a neuromodulatory target as it regulates various inflammatory processes including cytokine production, immune cell migration and proliferation. When evaluating the CB2 receptor expression in PD, it's been reported to be upregulated in the substantia nigra of PD patients by immunohistochemical (8, 9) and transcriptional measures (10). Similarly, it has been found increased in mouse models of nigral degeneration (11, 12). Evidence from several groups has demonstrated that overexpressing CB2 or pharmacologically targeting the receptor in neurotoxin animal models of PD results in dampened inflammation and in some cases neuroprotection(13, 14). Non-selective cannabinoid receptor agonists have also found to benefit neurotoxin-induced neuroinflammation and neurodegeneration in PD animal models (11, 15). Yet, only one report, using genetic deletion approaches, has evaluated the role of CB2 on the clearance of Asyn aggregates (16). There has not yet been a study to evaluate CB2-selective ligands on Asyn burden *in vivo*.

To further understand the role of CB2 in Asyn clearance, we sought to determine the effects of peripheral treatment with a novel CB2 inverse agonist, SMM-189, on Asyn-induced pathologies in a rat model of viral vector-driven Asyn overexpression. Previous studies using SMM-189 demonstrated immunomodulatory effects that improve acute neuronal injury and behavioral outcomes in TBI models potentially explained by a mechanism that suppresses pro-inflammatory markers and increases anti-inflammatory effects (17-19). Inverse agonists bind constitutively-active CB2 receptors and lock them into an inactive conformation state preventing coupling to $G_{\alpha i/o}$ with a concomitant increase in cyclic AMP (cAMP) production (20). SMM-189 has microglial effects on this canonical pathway as previously shown by increased levels of nuclear phosphorylated cAMP response-element binding protein (pCREB), triggering downstream transcription of wound-healing cytokines (21). Therefore, we hypothesize that targeting CB2 will promote clearance of Asyn by altering the central inflammatory environment. In this study, we provide evidence that pharmacological inverse agonism of CB2 alters the inflammatory state of peripheral and central immune cells and reduces levels of phosphorylated human Asyn in the brain.

Methods

Animals

Sprague Dawley male rats (16-18 weeks of age, 400-525g) were purchased from *Charles River Laboratories* and acclimated to Emory University animal facilities. Rats were pair housed in standard plexiglass cages under normal 12-hr light cycles. Two cohorts of rats were administered unilateral stereotaxic injections of AAV2/5-human wild-type Asyn (2.9 – 4.3 x 10^{11} vg/mL provided by Dr. Manfredsson) into the left nigra at coordinates AP -5.3 mm, ML +2.0 mm, DV -7.2 mm and AP -6.0 mm, ML +2.0 mm, and DV -7.2 mm using a glass capillary needle fitted to a Hamilton syringe. This titer was previously shown to not induce nigral neurotoxicity (22), thereby generating a model with overexpression of human wild-type Asyn and Asyn-mediated neuroinflammation. One week after surgery, animals were randomly selected to receive daily systemic injections of either SMM-189 (i.p., 6 mg/kg, cohort 1: n=14; cohort 2: n=6) or vehicle (cohort 1: n=14; cohort 2: n=5) and followed for 8 weeks (**Figure 1**). Plasma was collected at baseline and every 2-4 weeks post-AAV-hAsyn injections to measure levels of SMM-189. Rats were housed and handled in accordance with protocols approved by the IACUC of Emory University. At sacrifice, animals were transcardially perfused with ice-cold PBS and the frontal cortex frozen for RNA analysis, the striatum frozen for western analysis, and the midbrain post-fixated in 4% PFA to be processed for immunohistochemistry. Additionally, PBMCs were isolated from blood and analyzed at endpoint for gene expression changes using qPCR analysis. The second cohort of rats was added to perform additional immunohistochemical analyses.

An additional cohort of rats ("high-titer" cohort) was evaluated to determine effects of SMM-189 on immune cell populations in the brain and periphery (**Figure 1**). To ensure infiltrating peripheral immune cells, rats were stereotaxically injected with a higher titer of AAV2/5-human wild-type Asyn (4.6E12 vg/mL provided by Dr. Manfredsson) and underwent an identical drug treatment timeline with animals sacrificed at 4 (SMM-189: n=5; vehicle: n=6) and 8 weeks (SMM-189: n= 7; vehicle: n=7). PBMCs were isolated from blood at baseline, 4 and 8 weeks after stereotaxic surgery and immunophenotyped using flow cytometry. Brains were collected at endpoint, brain immune cells isolated and evaluated using multi-color flow cytometry.

SMM-189 formulation

SMM-189 was provided by Dr. Bob Moore III and formulated with 15% ethanol (v/v), 15% cremophor (w/v) and 70% saline (v/v). In brief, SMM-189 was dissolved in 15% ethanol, cremophor was weighed in a separate vial and dissolved SMM-189 slowly added and mixed gently until combined. Saline was slowly added and mixed until achieving a homogenous solution. The final solution was sterile filtered with a syringe 0.22µm filter and stored at 4°C in amber sterile-glass vials for up to 2 weeks. Vehicle treatments consisted of the same concentrations of ethanol, cremophor and saline. Daily injections were administered by research staff blinded to treatment history.

Blood and CSF collection

Blood was collected from the tail vein at baseline and every 2-4 weeks post-AAV (cohort 1: ~18-20 hours post-drug injection; cohort 2 and high-titer: ~2 hours post-drug injection) for plasma to measure SMM-189 levels. Animals were placed in an induction box and anesthetized with 3% isofluorane and maintained on 1-2% isofluorane for the remainder of the procedure. Tails were

cleaned with ethanol and approximately 400uL of blood drawn was drawn for the lateral tail vein. Body temperature was maintained using a heating pad. Blood was collected from rats in the high-titer cohort in a similar manner at baseline, 4 and 8 weeks post stereotaxic surgery and PBMCs isolated for multi-color flow cytometry.

CSF was collected at endpoint from cohort 2. In brief, rats were placed in a stereotaxic frame and the head fixed downwards. An incision was made to expose the muscle layer over the cisterna magna. A sterile pulled micropipettes attached to tubing and a syringe punctured into the cisterna magna and clean CSF was aspirated and collected in a 0.2mL Eppendorf and stored at -80°C.

Mass Spectrometry and Assessment of of SMM-189 in Plasma and CSF

SMM-189 and d^5-SMM-189 were synthesized as previously described (23). A total of 50 µL aliquots of plasma or CSF were prepared by protein precipitation with 100 µL acetonitrile (spiked with the internal standard d^5-SMM-189) followed by centrifugation at 10,000*g* for 10 min at 4°C. Chromatographic separation of the supernatant was performed using a Zorbax SB-C18 3.5 µm 4.6x150 mm and a Shimadzu HPLC Nexera XR with Solvent Delivery Module LC-20ADXR, CTO-20AC prominence column oven (temperature 40°C), a DGU-20A5R Degassing Unit, and a SIL-20ACXR autosampler. The aqueous mobile phase (A) was 95% water and 5% acetonitrile (B) was 100% acetonitrile. The flow rate was set to 500 µL/min and the gradient elution initial 50% B, 0.5 to 3min 50% to 100%B, 6 to 6.1min 100% to 50% B, 6.5min stop with a column wash using methanol:water (1:1). Sample analysis was performed using SCIEX Triple Quad 5500 tandem mass spectrometer (Framingham, MA) operated in the negative ion mode at ion spray voltage -4500V and temperature 600°C. Multiple reaction monitoring mode using the compound-specific mass transfers of m/z 357 → 185 for SMM-189, and m/z 362 → 185 for d^5-SMM-189 was used for analysis. A calibration curve ranging from 1 to 100 ng/mL was constructed and validated with spiked samples of rat plasma. The peak area ratios of analyte to the internal standard were linear over the tested concentration range.

Blood Brain Barrier Penetration of SMM-189

Analysis of the brain-to-blood ratios of SMM-189 were performed by Sai Life Sciences Limited (Telangana, India). All procedures of the study were in accordance with the guidelines provided by the Committee for the Purpose of Control and Supervision of Experiments on Animals (CPCSEA) as published in The Gazette of India, December 15, 1998. Prior approval of the Institutional Animal Ethics Committee (IAEC) was obtained before initiation of the study. In brief, 54 mice were weighed and divided as Group 1 (6 mg/kg, i.p.) and Group 2 (6 mg/kg, p.o.). Animals in Group 1 and Group 2 were administered intraperitoneally and orally with SMM-189 solution formulation at 6 mg/kg in 5% Ethanol, 5% Cremophor and 90% Normal Saline, respectively. The blood samples were collected under light isoflurane anesthesia at 0.08, 0.25, 0.5, 1, 2, 4, 8, 12 and 24 hr (i.p.) and 0.25, 0.5, 1, 2, 4, 6, 8, 12 and 24 hr (p.o.) in labeled micro centrifuge tube containing K_2EDTA as anticoagulant. After blood collection, plasma was harvested by centrifugation and stored at -70 ºC until analysis. Immediately after collection of blood, Brain samples were collected from set of three mice at each time point at 0.08, 0.25, 0.5, 1, 2, 4, 8, 12 and 24 hr (Group 1; i.p.) and 0.25, 0.5, 1, 2, 4, 6, 8, 12 and 24 hr (Group 2; p.o.). Brain samples were homogenized using ice-cold phosphate buffer saline (pH-7.4) in a ratio of 2 (buffer):1(brain); and homogenates were stored below -70±10 ºC until analysis. Total homogenate volume was three times the brain weight. All samples were processed for analysis by protein precipitation

using acetonitrile and analyzed with fit-for-purpose LC-MS/MS method (LLOQ = 1.02 ng/mL for plasma and 6.09 ng/g for Brain).

Non-compartmental-analysis module in Phoenix WinNonlin® (Version 6.3) was used to assess the pharmacokinetic parameters. Maximum concentration (Cmax) and time to reach the maximum concentration (Tmax) were the observed values. The areas under the concentration time curve (AUClast and AUCinf) were calculated by linear trapezoidal rule. The terminal elimination rate constant, k_e was determined by regression analysis of the linear terminal portion of the log plasma concentration-time curve. The terminal half-life (T1/2) was estimated as $0.693/k_e$.

Immune cell isolation

PBMCs were isolated from tail vein blood of rats in the high-titer cohort at baseline, 4 and 8 weeks after AAV2/5-human wild-type Asyn (or following 3 and 7 weeks of daily peripheral treatments). Cohort 1 (low-titer cohort) rats also had PBMCs isolated for qPCR analysis of immune genes. Red blood cells were lysed using 1x RBC lysis buffer (Biolegend, 420301) for 5 minutes in the dark. Lysis buffer was neutralized by adding 1x HBSS (Gibco, 14175095). Cells were pelleted by centrifugation at 400*g* for 5 minutes, supernatant removed, and cells washed with HBSS. For the high-titer cohort, cells were resuspended in 200uL of PBS and transferred to a 96-well v-bottom plate for flow cytometry staining. For cohort 1, 10,000 cells were lysed in 600uL RLT lysis buffer + 1% BME, centrifuged through QiaShredder (2 minutes at 21,130gRPM). Lysate was then stored at -80°C and later processed for RNA extraction.

Brains were collected from animals in the high-titer cohort at either 4 or 8 weeks after AAV2/5-human wild-type Asyn (or following 3 and 7 weeks of daily peripheral SMM189 or vehicle treatments) and brain immune cells were isolated from each hemisphere. Hemispheres were finely cut in RPMI 1640 media (Gibco, 11875-093) with a scalpel blade and enzymatically dissociated with collagenase VIII (1.4U/mL; Sigma C2139), DNAse1 (1mg/mL; Sigma DN25) in 37°C for 15 minutes. Enzymes were neutralized with 10%FBS in RPMI 1640 complete media and centrifuged 400*g* at room temperature. Tissue was resuspended in 1x HBSS and mechanically dissociated using a Pasteur pipette until a cell suspension was generated. The suspension was passed through a 70µM cell strainer and strainers rinsed twice with 1x HBSS. To remove myelin, the strained suspension was centrifuged at 300*g* at 4°C for 5 minutes and resuspended in 37% percoll and layered between 70% and 30% percoll gradients. The samples were centrifuged at 400*g* for 30 minutes at room temperature with the brake disabled. The top myelin layer was aspirated and demyelinated immune cells were collected from the 37% and 70% percoll interface with a pipette and washed with 1x HBSS twice, resuspended in PBS and placed in a 96-well v-bottom plate for flow cytometry staining.

Multiplexed Immunoassays

Plasma and CSF were analyzed for cytokines IFN, IL-10, IL-1B, IL-4, IL-6, and TNF using a custom V-PLEX Proinflammatory panel (K153AOH, MesoScaleDiscovery, MSD) and diluted with homogenization buffer at 1:4 for plasma and 1:1 for CSF. All biofluids were measured in duplicate and immunoassays performed on the MSD 1300 Meso Quickplex imager as per the manufacturer’s instructions by a researcher blinded to treatment history at the Emory Multiplexed Immunoassay Core (EMIC).

RNA extraction and qPCR

Total RNA was extracted from the frontal cortex and from PBMCs of cohort 1 and standardized across all samples and groups (24). In short, tissue was suspended in Trizol and homogenized with a TissueLyser (Retsch). Homogenate was incubated with chloroform and RNA separated by centrifugation of 113,523gfor 15 minutes at 4°C. RNA was further isolated with a RNAeasy mini kit (Qiagen). The RNA (1μg) was then reverse transcribed to cDNA and analyzed with primers (Integrated DNA Technologies) for pro-inflammatory and anti-inflammatory immune markers and CB2 (**Table 1**) by qRT-PCR using protocols previously published (24). Resulting threshold cycle (Ct) values were analyzed by the 2-ΔΔCt method using the AAV2/5-hαsyn + vehicle as the control group and normalized to GAPDH for PBMCs and HPRT1 for frontal cortex as the housekeeping genes.

Multicolor flow cytometry

Peripheral and central immune cell staining was performed similar to previously published protocols (25). In brief, immune cells were washed and resuspended in PBS, then incubated for 30 minutes at room temperature in LIVE/DEAD Fixable Red Dead cell stain (ThermoFisher Scientific, L23102; 1:2000). Following two washes in PBS, Fc receptors were blocked with anti-rat CD32 Fc block diluted 1:100 in FACS buffer (1mM EDTA and 0.1% sodium azide in PBS) for 15 minutes at 4°C. PBMCs were incubated with separate myeloid and lymphoid panels and brain immune cells incubated with an antibody panel to identify microglia, monocytes and lymphocytes (**Table S1-3**). Fluorophore conjugated antibodies diluted with FACS buffer were incubated at 4°C for 20 minutes. Cells stained for surface myeloid markers were fixed in 1% PFA for 25 minutes and washed in FACS. Cells stained with lymphoid panel antibodies followed a protocol for intracellular staining of transcriptional marker Foxp3. Here, cells were incubated for 30 minutes in fixation/permeabilization working solution (eBioscience 00-5523-00), washed in 1x permeabilization buffer, additionally blocked with 2% mouse serum for 15 minutes and anti-rat foxp3-AF647 added to block for an additional 30-minute incubation. Immune cells stained with the lymphoid panel were then washed and resuspended in FACs buffer. All cells had 10uL of AccuCheck Counting beads (ThermoFisher, PCB100) added to final suspension and cells were run on a LSRII Instrument (BD Biosciences, Franklin Lakes, NJ) with FACSDiva software (BD Biosciences). Results were analyzed using FlowJo 10.8.1 software and populations of monocytes (classical and non-classical), lymphocytes (CD4+ and CD8+) or microglia defined by specific gating strategies (**Figure S1-S3**)(26-28). For PBMC analysis, raw frequencies were normalized across serial runs against vehicle-treated values using the following equation: Raw frequency / (average vehicle frequencies of specific run / average baseline frequencies). For brain immune cell analysis, frequencies were normalized across treatment group at each timepoint using the following equation: raw frequency / (average treatment frequency of specific run 1 / average treatment frequency of specific run 2).

Immunohistochemistry

Brains were post-fixed in 4%PFA for 48 hours and transferred to 30% sucrose and cut at 40μm on a freezing microtome. Immunohistochemical stains were performed as previously published with antibodies listed in **Table S4** (29). In brief, endogenous peroxidase was quenched with 3% hydrogen peroxide, blocked with 8% normal serum, avidin (Vector SP-2001) and 0.1% Triton-X and incubated overnight at 4°C with primary antibodies specific for alpha-synuclein (Clone

4B12; Biolegend 807801), pSer129 alpha-synuclein (Clone EP1536Y; Abcam AB51253), CD68 (Serotec MCA341R), MHCII (Biorad MCA46GA). Tissue was incubated in appropriate biotinylated secondary antibodies (pre-absorbed anti-mouse secondary), amplified with ABC (Vectastain PK-6100) and developed with diaminobenzidine tablets or diaminobenzidine drop kit with nickel (Vector SK-4100) for CD68 immunostaining.

Immunofluorescence

Tissue was blocked with 5% normal serum in TBS + Triton-X and further incubated overnight at 4°C with primary antibodies specific for IBA1 (Wako 019-19741) and tyrosine hydroxylase (Immunostar 22941) to identify microglia in the substantia nigra or tyrosine hydroxylase (Millipore AB152) and alpha-synuclein (Clone 4B12; biolegend 807801) to evaluate accuracy of stereotaxic injection targets. Tissue was incubated in secondary antibodies conjugated to appropriate fluorophores for 2 hours at room temperature and mounted tissue with aqueous mounting media with DAPI (Vectashield H-2000).

Histological analysis and quantification

Animals were assessed by an experimenter blinded to the treatment history for rigorous and proper assessment of unilateral targeting of AAV2/5-human wild-type Asyn into the SN using immunofluorescent analysis of human synuclein and tyrosine hydroxylase (**Figure S4**). Animals were excluded from analysis when poor stereotaxic targeting occurred, including missing human Asyn expression throughout the rostral-caudal axis of the SN or if expression was seen only in lateral SN. Six animals were excluded in total with the group size of SMM-189-treated cohort 1: n=12; cohort 2: n=6 and vehicle-treated cohort 1: n=12; cohort 2: n=3.

IBA1-positive total immune cell counts and area of immunoreactivity were quantified using Nikon NIS elements software. Four fluorescent z-stacks of IBA1 stained nigra were collected from images of lesioned and non-lesioned nigra from cohort 1 using a Nikon Eclipse 90i microscope and maximum project images were used for quantification. CD68-ir and CD163-ir was quantified from two to three microphotographs from each animal throughout the substantia nigra using ImageJ particle count analysis (30). Microphotographs of the nigra immunochemically stained for either Asyn, pSer129 Asyn and proteinase K-resistant Asyn were quantified using Image J (version 1.54f). Regions of Interest (ROIs) were drawn on two to three images throughout the nigra and optical density measurements collected and averaged for each animal. Measurements were normalized to the vehicle group so that data from all cohorts could be combined.

SDS-PAGE and immunoblotting

Striatal tissue from successfully targeted cohort 1 and cohort 2 rats was homogenized in ice-cold TriZOL lysed using the TissueLyser system. Homogenates were incubated with 20% chloroform and centrifuged at 13,523*g* for 15minutes at 4°C. Protein pellets were washed in methanol twice and resuspended in 1% SDS and heated to 50°C. Total protein concentrations were measured using Pierce BCA Protein Assay Kit and equal amount of protein (10-20µg) mixed with Laemmli sample buffer were loaded in 4-20% TGX precast gels (Biorad) for gel electrophoresis. Protein was transferred to a PVDF membrane (Biorad) using a Trans Blot Turbo Transfer System, the immunoblots were immediately fixed with 0.4% paraformaldehyde (PFA) for 30

minutes and stained for total protein using Revert 700 (Licor) for reliable normalization. Revert staining was captured and measured on the Licor Odyssey at 700nm for 30 seconds.

Non-specific protein binding was blocked with 5% milk and 0.1% Tween-20 in TBS for 1 hour at room temperature, and membranes incubated with primary antibodies overnight at 4°C. The blots were washed with 0.1%TBS-Tween-20, incubated with appropriate horseradish peroxidase-conjugated secondary antibodies (1:2000) at room temperature for 1 hour and developed with SuperSignal West Femto Enhancer or Pico Peroxide solutions under a chemiluminescent detection imaging system (Licor Odyssey). The density of the band was quantified using StudioLite software. Relative expression levels were normalized to its own total protein and to vehicle average expression level.

In vitro cell culture

The RAW264.7 macrophage cells were grown in sterile media which consisted of DMEM high glucose, 10% FBS, 2mM L-glutamine, 1x Pen-strep and 1x sodium pyruvate in a humidified 5% CO2 incubator at 37°C. RAW264.7 were maintained in 75cm^3 tissue culture flasks and plated at a density of 1x10^4 cells in triplicate in 96-well plates for assays. Cells were stimulated with either lipopolysaccharide (LPS O111:B4; Sigma L2630) at 100ng/mL or 1000ng/mL (750EU/mL or 7500 EU/mL, respectively). One hour prior to this stimulation the cells were pre-treated with the CB2 inverse agonist SMM-189 at 3uM or 7uM or its vehicle. Specifically for cell culture experiments, SMM-189 was formulated with 40% ethanol (v/v), 20% tween-20 (v/v) and 40% saline (v/v). A phagocytosis assay was conducted 24 hours after LPS.

Phagocytosis assay

The phagocytosis assay was performed using pHrodo green *E. coli* bioparticles (Invitrogen cat. P35366) according to the manufacturer's instructions. Five images per well were then collected every 30 minutes for 24 hours on an EVOS M7000 microscope (Invitrogen, ThermoFisher Scientific). The cells were maintained for this duration using an on-stage incubator kept at 37°C and 5% CO_2. Analysis of the collected images was performed using EVOS Celleste software (version 5.0), which counted the cells and then measured the integrated optical density of fluorescence within each well over the 24-hour time course. Analysis was conducted on the average integrated optical density across triplicate wells. Results were consistent across duplicate experimental replicates.

Statistics

Statistical analysis was conducted using GraphPad Prism software (version9.5.1). *In vivo* histological, western and transcriptional analyses were analyzed using parametric unpaired t-tests to determine the statistical difference between SMM-189 and vehicle-treated groups. When both cohort 1 and 2 were included in the analysis, the data was normalized to the vehicle-treated group within that cohort. Flow cytometry data of brain immune cells was analyzed using a two-way ANOVA (factors of hemisphere and treatment) and multiple comparisons performed using uncorrected Fishers LSD, while PBMC serial flow data was analyzed using a fixed-effect model (factors of time and treatment) and multiple comparisons performed using uncorrected Fishers LSD. Cell experiments were analyzed using a one-way ANOVA to determine differences between treatment groups across the entire timed experiment using a Dunnet's multiple comparison test.

Results

Phosphorylated Asyn in substantia nigra is decreased by SMM-189 treatment

To assess the effect of SMM-189 on alpha-synuclein aggregation, midbrains from the low titer cohort were immunohistochemically stained for human phosphorylated (pS129) Asyn (clone EP1536Y; abcam ab512253). This phosphorylation site is pathologically relevant as it has been found in Lewy bodies in postmortem samples (31, 32) and has been shown to accelerate aggregation of alpha-synuclein in vitro and in vivo (33, 34), suggesting that pS129 is linked to aggregation. Optical density analysis of the substantia nigra revealed reduced pS129-immunoreactivity in SMM-189-treated animals when normalized against vehicle-treated animals ($t(23)=3.353$, $p=0.0023$; **Figure 2A,B**). Striatum protein ipsilateral to the overexpression of human alpha-synuclein was evaluated using western analysis and similarly demonstrated reduced pS129 levels in SMM-189-treated rats ($t(15)=3.710$, $p=0.0021$; **Figure 2G,H**). Total and proteinase-K resistant Asyn was also evaluated in the substantia nigra and found that while levels of total Asyn (Biolegend, clone 4B12) were not different between treatments, SMM-189 produced a trend to reduced PK resistant alpha-synuclein compared to vehicle across cohorts 1 and 2 ($t(20)=1.829$, $p=0.0824$; **Figure 2C-F**) when normalized to vehicle nigra measurements. Consistent with histological analyses of total Asyn in the nigra, the striatum total human Asyn levels were not different between treatments as determined by western analysis (**Figure 2G-H**).

SMM-189 measurements in CSF confirmed penetration into rat brain

Next, we evaluated the levels of SMM-189 from plasma of rats from both cohorts 1 and 2 and the high-titer cohort. Significant increases were detected in the level of plasma SMM-189 in animals receiving SMM-189 treatment in cohort 2 (treatment $F(1,9)=29.62$, $p=0.0004$; time $F(2,18) = 15.29$, $p=0.0001$) at 4 ($p=0.0016$) and 8 weeks ($p<0.0001$) compared to vehicle-treated rats (**Figure S5C,D**). Similarly, cohort 1 SMM-189 plasma levels increased with time ($F(1.162,15.11)$, $p=0.0207$) compared to baseline levels at 2 ($p=0.0087$), 4 ($p=0.0464$) and 8 weeks ($p=0.0061$; **Figure S5A,B**). Levels of SMM-189 remained low in the CSF with an average of 0.44±0.22SEM ng/mL (**Figure S5E**) and a brain to plasma ratio average of 0.032±0.02SEM. This is in contrast to the brain to plasma ratios measured for SMM-189 in murine PK studies wherein the brain to plasma ratio of SMM-189 was 0.74 following i.p. injection and 1.63 after p.o. administration (**Table 2**). Low levels of drug in the CSF is presumed to reflect the extensive portioning of SMM-189 (clogP value of ~5.26) into the brain tissue based on high penetration measured in murine PK studies. CSF was not collected from cohort 1 rats. Rats weight increased overtime ($p<0.0001$) as expected in both cohorts 1 and 2 with no significant differences between treatment groups. Similar plasma SMM-189 detectable levels and weight health were seen in the high-titer cohort (**Figure S5F,G**).

SMM-189 promotes an anti-inflammatory environment and shifts immune cell gene expression toward a wound healing phenotype in the CNS

To evaluate the effects of CB2 modulation on neuroinflammation, nigral sections were immunohistochemically examined for immune cell markers. SMM-189 did not change microglial IBA1+ numbers or area (**Figure 3A-D**). IBA1 analysis demonstrated lesion effects with significantly increased counts ($F(1,22)=18.72$, $p=0.003$) and area ($F(1,22)=22.94$, $p<0.0001$) in the Asyn-lesioned nigra compared to the non-injected side. Notably, the lesion effect on IBA1 was lessened in SMM-189-treated rats compared to vehicle-treated rats,

potentially highlighting the ability for SMM-189 to dampen Asyn-activated IBA1+ brain myeloid cells. In the striatum, western blot analysis revealed no differences in myeloid marker IBA1 and astrocyte marker GFAP expression levels across treatments (**Figure S6**). SMM-189 did promote an anti-inflammatory environment with increased nigral CD68-immunoreactive particle counts ($t(15)=3.413$, $p=0.0039$) in the substantia nigra injected with AAV-wt-hAsyn compared to vehicle treated conditions (**Figure 3E-G**). CD68 is a lysosomal marker and often a surrogate marker for phagocytic innate immune cells, suggesting an increase in phagocytic wound-healing cells in SMM-189-treated brains. CD163, an innate-immune marker identifying cells from the monocyte/macrophage lineage, was also histologically evaluated in the nigra and found to be decreased in SMM-189-treated rats compared to vehicle-treated animals ($t(7)=5.172$, $p=0.0013$).

To further assess inflammation, cytokines were evaluated from cohort 1 in the CSF and plasma and transcript levels determined from frontal cortex brain tissue and PBMCs by qRTPCR. No significant differences were detected between treatments in the CSF and plasma (**Figure S7**), however SMM-189 increased M2 alternative activation markers YM1 and CD206 gene expression in the frontal cortex and TGFβ in PBMCs relative to vehicle-treated animals (**Figure 3H,I**). Endpoint PBMCs also demonstrated decreased pro-inflammatory cytokine TNF transcript after SMM-189 treatment. CB2 gene expression was not different between groups confirming that the target is present in immune cells and brain.

SMM-189 induced significant time-dependent alterations in brain infiltrating immune cells and in peripheral monocyte populations

Next, to investigate the effects of SMM-189 on the infiltration of immune cells from the periphery, brain immune cells were isolated from the high-titer cohort by enzymatic digestion and percoll gradient separation at both 4- and 8-weeks post-treatment. Flow cytometry analysis at 4 weeks (**Figure 4**) revealed that SMM-189 treatment globally reduced CD172a+CD11b+ monocyte frequency (treatment: $F(1,20)=8.899$, $p=0.0073$) with significantly less monocyte infiltrates in the non-lesioned hemisphere as determined by multiple comparisons. Furthermore, no significant changes were detected in more defined classical or non-classical monocyte subset frequencies. However, CD43- classical monocytes displayed reduced mean fluorescent intensity (MFI) of the inhibitory marker ("do not eat me" signal) CD172a (treatment: $F(1,19)=4.552$, $p=0.0461$), with similar reductions in the activation marker CD11b found on microglia within the non-lesioned hemisphere of SMM-189-treated compared to vehicle-treated animals ($p=0.0241$). Frequencies of CD4+ T cells were also found to be reduced by SMM-189 treatment 4 weeks after AAV2/5-human wild-type Asyn injections. Although CD8 T cell frequencies were not significantly different, the CD4 to CD8 ratio was found to be decreased at 4 weeks in brains exposed to SMM-189.

Interestingly, 8 weeks after AAV injections, SMM-189 shifted brain immune cells frequencies in the opposite manner than at 4 weeks (**Figure 5**), such that CD172a+CD11b+ monocyte frequency was elevated in the lesioned hemisphere from SMM-189 treatment compared to vehicle (treatment: $F(1,24)=8.767$, $p=0.0068$). Additionally, increases were found in the frequency of antigen-presenting MHCII+ classical monocytes (treatment: $F(1,24)=5.703$, $p=0.0252$) with significant increase from multiple comparisons found in the presence of Asyn

(p=0.0213) and in the MFI of activation maker CD11b on microglia (treatment: F(1,24)=7.611, p=0.0109) with significant elevation in the non-lesioned hemisphere (p=0.0162). Furthermore, independent of the presence of Asyn, CD4+ lymphocytes globally increased (treatment: F(1,24)=14.33, p=0.0009), while CD8+ lymphocytes decreased (treatment: F(1,24)=18.15, p=0.0003) in SMM-189-treated animal brains compared to vehicle. Of note and consistent with immunohistochemical results, significant reductions in macrophage frequencies, identified as CD43-/CD163+, was found at 8 weeks following SMM-189 **(**treatment: F(1,24)=8.917, p=0.0064), with *post hoc* analysis indicating a significant reduction of macrophages in the lesioned hemisphere (p=0.0146).

In the periphery, SMM-189 reduced circulating classically-activated monocytes (CD43-His48+) as determined by flow cytometry **(**treatment: F(1,26)=4.75, p=0.0386) with a multiple comparisons demonstrating a significant decrease at 8 weeks in PBMCs of SMM-189-treated rats compared to vehicle-treated animals (p=0.0316). Furthermore, increases in the wound-healing non-classical monocytes (CD43+), which circulate and patrol in search of injury, was found in SMM-189 compared to vehicle at 8 weeks using multiple comparisons analysis (p=0.0493) (**Figure 6**). Lymphocyte frequencies of PBMCs did not reveal significant differences in CD4 or CD8 populations between treatments, however, animals treated with SMM-189 had elevated levels of Tregs (CD4+Foxp3+ and CD4+Foxp3+CD25+) at 8 weeks compared to their own baseline frequencies (**Figure S3**).

SMM-189 pretreatment enhances LPS-induced phagocytosis of RAW264.7 macrophages

To better understand the effects of SMM-189 on functional uptake and degradation by innate immune cells, a phagocytosis assay was performed using *E. coli* phHrodo bioparticles on RAW264.7 macrophage cells. SMM-189 potentiated the LPS-stimulated response as measured by the increased optical density of GFP expressed in the RAW cells (**Figure 7**). Specifically, when stimulated with 100ng/mL LPS there was a dose dependent response to SMM-189 where pre-treatment with either 3uM or 7uM significantly increased the integrated density of GFP when compared to pre-treatment with vehicle (p=0.0024, p<0.0001, respectively; **Figure 7A**). However, when stimulated with a higher concentration of LPS (1 ug/mL), both 3uM and 7uM doses of SMM-189 intensified phagocytosis of *E. coli* bioparticles compared to vehicle (p<0.0001 and p<0.0001, respectively; **Figure 7B**), suggesting a ceiling effect when cells are highly active. Regardless of LPS dose stimulation, GFP expression was significantly restricted with the additional incubation of cytochalasin D, an actin polymerization inhibitor.

Discussion

Evidence of chronic neuroinflammation and dysfunction of the innate immune system have been described in PD, which has given rise to a growing landscape of therapeutic interventions that target microglia and the peripheral immune system to delay or prevent disease progression (35). The cannabinoid system has become a recent target of interest due to its influence on the immune system and the increased legalization across continents of cannabis that directly acts on the cannabinoid receptors. Given the untoward side effects of cannabis intake on psychomotor performance, focus on the immunomodulatory CB2 signaling arm of the pathway represents a more desirable therapeutic game-changer for the field. The results of the present study demonstrate CB2 inverse agonism reduces toxic Asyn phosphorylation and aggregates and shifts central and peripheral immune cells toward a wound-healing, phagocytic phenotype in an Asyn rat model of nigral degeneration. These novel results point to a critical role of CB2 to mediate the function of brain immune cells to alter synucleinopathies.

Our IHC finding that SMM-189 treatment increased CD68-ir particles in the brain and reduced human phosphorylated Asyn suggests that brain myeloid immune cells such as microglia shifted toward a wound-healing phenotype that enabled them to phagocytose toxic Asyn aggregates better. Although this is the first study to evaluate the effects of a CB2-selective ligand on synucleiopathy, our results are in line with published studies that demonstrate CB2-deficient mouse models have reduced protein aggregation likely resulting from altered functions of microglia. Specifically, CB2 deficiency significantly decreased Amyloid-β plaque density in the hippocampus and improved cognitive and learning deficits in mouse models of Alzheimer's disease-like pathology (36, 37), suggesting that CB2 has a role in the removal of aggregated proteins. However, another study by Feng and colleagues evaluated CB2-deficient mice versus CB2 wild-type mice treated with human Asyn pre-formed fibrils (PFF) in the nucleus accumbens and found impaired Asyn clearance in the absence of CB2 (16). More specifically, they evaluated total Asyn area by immunofluorescence at four different timepoints over 24 hours after injections of PFF and found that CB2-deficient mice had elevated levels of Asyn area 2 hours after injection compared to wild-type mice. These opposing results could highlight the ability of CB2 deficient microglia to differentially degrade Amyloid-β versus Asyn or could relate to the number of residing microglia in the different evaluated brain regions. Our novel findings demonstrated that daily pharmacologic inverse agonism of CB2 significantly mitigates pSer129 Asyn and trended to reduce proteinase-K resistant Asyn, eight weeks after AAV injections. Multiple studies have identified phosphorylated Asyn to be critical for Asyn inclusion formation (34, 38), suggesting that the reduced pSer129 in this study may have overall therapeutic value. Feng and colleagues did not evaluate pSer129 in their study, but found elevated Asyn levels 2 hours after PFF injection. It is difficult to directly compare our Asyn results to this study because of the many differences in experimental design, but it is possible that the global genetic ablation of CB2 triggers compensatory mechanisms that influence the outcome and is not just a result of CB2 deficiency.

Our results support that CB2 plays a role in microglial response and phenotype. A previous study reported that CB2-deficient microglia display shorter projections that are less ramified within 24 hours after Asyn PFF injections relative to CB2 wild-type microglia as measured by a rigorous Scholl analysis (16). Although, we sampled adequately throughout the nigra, our data did not

show statistically significant differences in the size of IBA1+ cells when evaluated by IHC at 8 weeks, yet flow data do suggest that microglia were more activated at that timepoint as shown by the elevated CD11b expression. Importantly, consistent with our findings using CB2 inverse agonist treatment, Feng and colleagues similarly identified upregulated CD68+ microglia from the genetic ablation of CB2. Given that SMM-189 dampened microglial activation (reduced CD11b expression) and delayed monocyte infiltration in the brain at earlier timepoints (4 weeks) and then increased activation in both myeloid and lymphoid compartments at later timepoints (8 weeks), we conclude that CB2 modification can potentially lead to dynamic changes in microglial overtime.

Although this study demonstrated a neuroinflammatory response, the mechanism underlying this critical therapeutic effect have not been fully elucidated. Previous work has identified CB2-mediated cAMP/PKA signaling pathways including the phosphorylation of CREB to impact microglial phenotype (16, 21, 39). Additionally, recent reports explain that microglial transcription of CB2 is dependent on nuclear factor erythroid 2-related factor 2 (NRF2), a well-known regulator of redox homeostasis and inflammation (40). An antioxidant response element (ARE) sequence was recently found in the promoter region of the microglial CB2 (40). NRF2 binds ARE in the nucleus to initiate transcription, suggesting that CB2 is linked to microglia-specific NFR2 inflammatory signaling. We were not able to test the specific signaling of SMM-189 responsible for the microglial phenotype transformations. However, in future studies it will be necessary to evaluate the mechanisms of microglial CB2 modulation in the presence of a synucleionpathy as they may be time-dependent in a progressing model.

Our flow cytometry analyses revealed SMM-189 decreased the extent of infiltrating monocytes and CD4+ T cells at 4 weeks following human Asyn overexpression. Others have shown that viral mediated overexpression of Asyn in the brain induces an influx of peripheral chemokine receptor 2 or CCR2+ immune cells into the degenerating area and that knocking out CCR2 or blocking monocyte infiltration is sufficient to protect against neuronal degeneration (41). In line with reduced infiltration, microglia isolated from SMM-189 treated mice were less activated at 4 weeks as measured by a reduced CD11b+ MFI. Together, these data suggest that SMM-189 can modify early microglial responses to insults such as Asyn overexpression. Interestingly, SMM-189 treatment led to a higher frequency of monocytes in the lesioned hemisphere at 8 weeks following human Asyn overexpression compared to vehicle treatment, suggesting SMM-189 delayed the resolution of monocyte infiltration in the lesioned hemisphere. Additionally, at this timepoint elevated levels of CD163+ macrophages were found in the lesioned hemisphere both by flow cytometry and by IHC. Expression of CD163 has been associated with border associated macrophage, which have been identified as the driving cells for immune cell recruitment and infiltration (42). The elevated CD163+ cells and heightened activation of brain immune cells at 8 weeks, including more CD11b+ expression on microglia and frequency of MHCII+ monocytes, is likely to have triggered the extravasation and increased presence of CD4+ helper cells and decreased CD8+ cytotoxic cells. The increased CD4 to CD8 ratio found in the brains of SMM-189-treated rats support an activated immune response that may have contributed to the reduced synuclein pathology. Previous reports have found that T cell adoptive transfer to immune deficient mice reduced phosphorylated Asyn after pre-form fibril injections, suggesting that T cells can have direct modulatory effects on Asyn toxicity (43). It is possible that CB2 modulation had direct effects on T cells as they also express the receptor and CB2-mediated activation of T

cells alter functions including proliferation and migration (44-46). Although our results did show changes in T cell frequencies in the brain, the peripheral CD4+ and CD8+ T cells frequency did not change. Therefore, our data supports the idea that SMM-189 altered brain myeloid cell functions to attract and activate lymphocytes with little effect on peripheral T cells directly. We were not able to measure subtypes of T cells to understand more specific effects on T cell phenotypes, with the exception of Tregs, a cell essential to regulating and suppressing immune cells.We found increased peripheral Tregs after 8 weeks of peripheral SMM-189 treatment compared to baseline (**SFigure 3**).

Peripheral treatment with CB2 inverse agonist SMM-189 had body wide effects that were independent of human Asyn overexpression. Through multiple comparison analysis, some of the immune effects are found in the non-lesioned hemisphere and not in the hemisphere overexpressing human Asyn. This is not surprising as intracerebral injections break the dura and disturb the entire brain immune homeostasis, which can affect immune cell infiltration throughout the brain, not just on the injected hemisphere. Furthermore, SMM-189 was administered peripherally and therefore could have widespread brain effects as demonstrated by immune gene expression changes in the frontal cortex, an area not overexpressing human Asyn (**Figure 3H**). Our peripheral flow data at 8 weeks revealed that SMM-189 skewed peripheral monocytes with decreased pro-inflammatory CD43-His48+ classical monocytes and increased wound healing CD43+ non-classical monocytes. Although neither specific subset of monocytes was significantly altered in the brain, the shift in microglial phenotypes may have increased the amount of CCL2 release leading to an overall elevated monocyte fraction in SMM-189 lesioned hemispheres. While plasma cytokine levels did not change as a result of CB2 modulation, there was a significant shift in immune phenotype based on PBMC gene expression, with decreased TNF and increased TGFβ which promotes alternative macrophage activation. These findings suggest that SMM-189 altered downstream CB2 signaling and promoted an anti-inflammatory brain microenvironment in the nigra that could not be captured when evaluating biofluids at a systems level.

Conclusion

The cannabinoid system has become a new and exciting target in PD and other neurological conditions (15). Recently, homozygous loss of function diacylglycerol-lipase beta (DAGLB) mutations were reported to be linked to early-onset PD in different families of Chinese descent (47). DAGLB synthesizes 2-Arachidonoylglycerol (2-AG), which is a potent brain endocannabinoid that has high potency for CB1 and CB2 receptors. Besides the recent genetic link to the cannabinoid system, others have identified protein expression of CB2 in brains of patients, underscoring the neuroanatomical basis for targeting CB2. Our novel findings demonstrate that CB2-selective inverse agonist with SMM-189 can alter immune responses both in the periphery and the brain to mitigate aggregation of toxic species of Asyn. To our knowledge, this is the first study to highlight CB2 as a promising therapeutic target for proteinopathies with notable accompanying neuroinflammation.

List of abbreviations

CB2, cannabinoid receptor 2
Asyn, alpha-synuclein
pSer129, phosphorylated serine 129 alpha-synuclein

PD, Parkinson's disease
LPS, lipopolysaccharide
PBMC, peripheral blood mononuclear cells
MFI, mean fluorescent intensity

Declarations

Ethics approval and consent to participate. Sprague Dawley rats were housed and handled in accordance with protocols approved by the IACUC of Emory University (protocol: DAR-2003358-ENTRPR-N). All surgeries and procedures including those under anesthesia were performed in IACUC approved settings at Emory University. Additionally, anesthesia and euthanasia procedures were conducted in accordance with the American Veterinary Medical Association Guidelines for the Euthanasia of animals and approved by Division of Animal Resources veterinarians at Emory. Analysis of the brain-to-blood ratios of SMM-189 were performed by Sai Life Sciences Limited (Telangana, India). All procedures of the study were in accordance with the guidelines provided by the Committee for the Purpose of Control and Supervision of Experiments on Animals (CPCSEA) as published in The Gazette of India, December 15, 1998. Prior approval of the Institutional Animal Ethics Committee (IAEC) was obtained before initiation of the study.

Consent for publication. Not applicable

Availability of data and materials. All data generated or analyzed during this study are included in this published article [and its supplementary information files]. Raw files can be provided upon request to the corresponding author.

Competing interests. The authors declare that they have no competing interests

Funding. Funding for this study was provided by the following: The Michael J Fox Foundation Target validation grant 2016 (MGT) and supplement (VJ), Graduate and Postdoctoral Training in Environmental Health Science and Toxicology T32ES012870 (VJ), Emory Udall Pilot grant 1P50NS098685 (VJ), Training in translational Research in Neurology 2T32NS007480-16 (VJ). Funding for the murine PK study was provided by a seed grant from the University of Tennessee Health Science Center (BMM).

Authors contributions

VJ and MGT conceived the study. VJ designed the study and supervised the technical staff involved in the study. VJ, FPM, BM, CM, DO, HS, JC, CAM, SG, SDK, MG, DL performed the various surgeries and assays. BMM provided guidance on drug dosing and study design. VJ, BMM, and MGT wrote and edited the paper. All authors reviewed and approved the final version of the manuscript.

Acknowledgements

We thank the Emory Flow Cytometry Core and Emory Multiplexed Immunoassay Core (EMIC) for their assistance with the use of the LSRII and performing MSD multi-plex immunoassays, respectively.

References

1. Uriarte Huarte O, Kyriakis D, Heurtaux T, Pires-Afonso Y, Grzyb K, Halder R, et al. Single-Cell Transcriptomics and In Situ Morphological Analyses Reveal Microglia Heterogeneity Across the Nigrostriatal Pathway. Front Immunol. 2021;12:639613.
2. Paolicelli RC, Sierra A, Stevens B, Tremblay ME, Aguzzi A, Ajami B, et al. Microglia states and nomenclature: A field at its crossroads. Neuron. 2022;110(21):3458-83.
3. Smajic S, Prada-Medina CA, Landoulsi Z, Ghelfi J, Delcambre S, Dietrich C, et al. Single-cell sequencing of human midbrain reveals glial activation and a Parkinson-specific neuronal state. Brain. 2022;145(3):964-78.
4. Joers V, Tansey MG, Mulas G, Carta AR. Microglial phenotypes in Parkinson's disease and animal models of the disease. Prog Neurobiol. 2017;155:57-75.
5. Ferreira SA, Romero-Ramos M. Microglia Response During Parkinson's Disease: Alpha-Synuclein Intervention. Front Cell Neurosci. 2018;12:247.
6. Earls RH, Menees KB, Chung J, Barber J, Gutekunst CA, Hazim MG, et al. Intrastriatal injection of preformed alpha-synuclein fibrils alters central and peripheral immune cell profiles in non-transgenic mice. J Neuroinflammation. 2019;16(1):250.
7. Ashton JC, Glass M. The cannabinoid CB2 receptor as a target for inflammation-dependent neurodegeneration. Curr Neuropharmacol. 2007;5(2):73-80.
8. Gomez-Galvez Y, Palomo-Garo C, Fernandez-Ruiz J, Garcia C. Potential of the cannabinoid CB(2) receptor as a pharmacological target against inflammation in Parkinson's disease. Prog Neuropsychopharmacol Biol Psychiatry. 2016;64:200-8.
9. Garcia MC, Cinquina V, Palomo-Garo C, Rabano A, Fernandez-Ruiz J. Identification of CB(2) receptors in human nigral neurons that degenerate in Parkinson's disease. Neurosci Lett. 2015;587:1-4.
10. Navarrete F, Garcia-Gutierrez MS, Aracil-Fernandez A, Lanciego JL, Manzanares J. Cannabinoid CB1 and CB2 Receptors, and Monoacylglycerol Lipase Gene Expression Alterations in the Basal Ganglia of Patients with Parkinson's Disease. Neurotherapeutics. 2018;15(2):459-69.
11. Price DA, Martinez AA, Seillier A, Koek W, Acosta Y, Fernandez E, et al. WIN55,212-2, a cannabinoid receptor agonist, protects against nigrostriatal cell loss in the 1-methyl-4-phenyl-1,2,3,6-tetrahydropyridine mouse model of Parkinson's disease. Eur J Neurosci. 2009;29(11):2177-86.
12. Garcia C, Palomo-Garo C, Garcia-Arencibia M, Ramos J, Pertwee R, Fernandez-Ruiz J. Symptom-relieving and neuroprotective effects of the phytocannabinoid Delta(9)-THCV in animal models of Parkinson's disease. Br J Pharmacol. 2011;163(7):1495-506.
13. Ternianov A, Perez-Ortiz JM, Solesio ME, Garcia-Gutierrez MS, Ortega-Alvaro A, Navarrete F, et al. Overexpression of CB2 cannabinoid receptors results in neuroprotection against behavioral and neurochemical alterations induced by intracaudate administration of 6-hydroxydopamine. Neurobiol Aging. 2012;33(2):421 e1-16.

14. Javed H, Azimullah S, Haque ME, Ojha SK. Cannabinoid Type 2 (CB2) Receptors Activation Protects against Oxidative Stress and Neuroinflammation Associated Dopaminergic Neurodegeneration in Rotenone Model of Parkinson's Disease. Front Neurosci. 2016;10:321.
15. Kelly R, Joers V, Tansey MG, McKernan DP, Dowd E. Microglial Phenotypes and Their Relationship to the Cannabinoid System: Therapeutic Implications for Parkinson's Disease. Molecules. 2020;25(3).
16. Feng L, Lo H, You H, Wu W, Cheng X, Xin J, et al. Loss of cannabinoid receptor 2 promotes alpha-Synuclein-induced microglial synaptic pruning in nucleus accumbens by modulating the pCREB-c-Fos signaling pathway and complement system. Exp Neurol. 2023;359:114230.
17. Reiner A, Heldt SA, Presley CS, Guley NH, Elberger AJ, Deng Y, et al. Motor, visual and emotional deficits in mice after closed-head mild traumatic brain injury are alleviated by the novel CB2 inverse agonist SMM-189. Int J Mol Sci. 2014;16(1):758-87.
18. Presley C, Abidi A, Suryawanshi S, Mustafa S, Meibohm B, Moore BM. Preclinical evaluation of SMM-189, a cannabinoid receptor 2-specific inverse agonist. Pharmacol Res Perspect. 2015;3(4):e00159.
19. Guley NM, Del Mar NA, Ragsdale T, Li C, Perry AM, Moore BM, et al. Amelioration of visual deficits and visual system pathology after mild TBI with the cannabinoid type-2 receptor inverse agonist SMM-189. Exp Eye Res. 2019;182:109-24.
20. Atwood BK, Wager-Miller J, Haskins C, Straiker A, Mackie K. Functional selectivity in CB(2) cannabinoid receptor signaling and regulation: implications for the therapeutic potential of CB(2) ligands. Mol Pharmacol. 2012;81(2):250-63.
21. Bu W, Ren H, Deng Y, Del Mar N, Guley NM, Moore BM, et al. Mild Traumatic Brain Injury Produces Neuron Loss That Can Be Rescued by Modulating Microglial Activation Using a CB2 Receptor Inverse Agonist. Front Neurosci. 2016;10:449.
22. Gombash SE, Manfredsson FP, Kemp CJ, Kuhn NC, Fleming SM, Egan AE, et al. Morphological and behavioral impact of AAV2/5-mediated overexpression of human wildtype alpha-synuclein in the rat nigrostriatal system. PLoS One. 2013;8(11):e81426.
23. Alghamdi SS, Mustafa SM, Moore Ii BM. Synthesis and biological evaluation of a ring analogs of the selective CB2 inverse agonist SMM-189. Bioorg Med Chem. 2021;33:116035.
24. MacPherson KP, Eidson LN, Houser MC, Weiss BE, Gollihue JL, Herrick MK, et al. Soluble TNF mediates amyloid-independent, diet-induced alterations to immune and neuronal functions in an Alzheimer's disease mouse model. Front Cell Neurosci. 2023;17:895017.
25. Houser MC, Uriarte Huarte O, Wallings RL, Keating CE, MacPherson KP, Herrick MK, et al. Progranulin loss results in sex-dependent dysregulation of the peripheral and central immune system. Front Immunol. 2022;13:1056417.
26. Barnett-Vanes A, Sharrock A, Birrell MA, Rankin S. A Single 9-Colour Flow Cytometric Method to Characterise Major Leukocyte Populations in the Rat: Validation in a Model of LPS-Induced Pulmonary Inflammation. PLoS One. 2016;11(1):e0142520.
27. Ahuja V, Miller SE, Howell DN. Identification of two subpopulations of rat monocytes expressing disparate molecular forms and quantities of CD43. Cell Immunol. 1995;163(1):59-69.
28. Kiefer J, Zeller J, Bogner B, Horbrand IA, Lang F, Deiss E, et al. An Unbiased Flow Cytometry-Based Approach to Assess Subset-Specific Circulating Monocyte Activation and Cytokine Profile in Whole Blood. Front Immunol. 2021;12:641224.

29. Houser MC, Caudle WM, Chang J, Kannarkat GT, Yang Y, Kelly SD, et al. Experimental colitis promotes sustained, sex-dependent, T-cell-associated neuroinflammation and parkinsonian neuropathology. Acta Neuropathol Commun. 2021;9(1):139.
30. Joers V, Masilamoni G, Kempf D, Weiss AR, Rotterman TM, Murray B, et al. Microglia, inflammation and gut microbiota responses in a progressive monkey model of Parkinson's disease: A case series. Neurobiol Dis. 2020;144:105027.
31. Fujiwara H, Hasegawa M, Dohmae N, Kawashima A, Masliah E, Goldberg MS, et al. alpha-Synuclein is phosphorylated in synucleinopathy lesions. Nat Cell Biol. 2002;4(2):160-4.
32. Anderson JP, Walker DE, Goldstein JM, de Laat R, Banducci K, Caccavello RJ, et al. Phosphorylation of Ser-129 is the dominant pathological modification of alpha-synuclein in familial and sporadic Lewy body disease. J Biol Chem. 2006;281(40):29739-52.
33. Smith WW, Margolis RL, Li X, Troncoso JC, Lee MK, Dawson VL, et al. Alpha-synuclein phosphorylation enhances eosinophilic cytoplasmic inclusion formation in SH-SY5Y cells. J Neurosci. 2005;25(23):5544-52.
34. Karampetsou M, Ardah MT, Semitekolou M, Polissidis A, Samiotaki M, Kalomoiri M, et al. Phosphorylated exogenous alpha-synuclein fibrils exacerbate pathology and induce neuronal dysfunction in mice. Sci Rep. 2017;7(1):16533.
35. Tansey MG, Wallings RL, Houser MC, Herrick MK, Keating CE, Joers V. Inflammation and immune dysfunction in Parkinson disease. Nat Rev Immunol. 2022;22(11):657-73.
36. Lopez A, Aparicio N, Pazos MR, Grande MT, Barreda-Manso MA, Benito-Cuesta I, et al. Cannabinoid CB(2) receptors in the mouse brain: relevance for Alzheimer's disease. J Neuroinflammation. 2018;15(1):158.
37. Schmole AC, Lundt R, Toporowski G, Hansen JN, Beins E, Halle A, et al. Cannabinoid Receptor 2-Deficiency Ameliorates Disease Symptoms in a Mouse Model with Alzheimer's Disease-Like Pathology. J Alzheimers Dis. 2018;64(2):379-92.
38. Lee KW, Chen W, Junn E, Im JY, Grosso H, Sonsalla PK, et al. Enhanced phosphatase activity attenuates alpha-synucleinopathy in a mouse model. J Neurosci. 2011;31(19):6963-71.
39. Tao Y, Li L, Jiang B, Feng Z, Yang L, Tang J, et al. Cannabinoid receptor-2 stimulation suppresses neuroinflammation by regulating microglial M1/M2 polarization through the cAMP/PKA pathway in an experimental GMH rat model. Brain Behav Immun. 2016;58:118-29.
40. Galan-Ganga M, Del Rio R, Jimenez-Moreno N, Diaz-Guerra M, Lastres-Becker I. Cannabinoid CB(2) Receptor Modulation by the Transcription Factor NRF2 is Specific in Microglial Cells. Cell Mol Neurobiol. 2020;40(1):167-77.
41. Harms AS, Thome AD, Yan Z, Schonhoff AM, Williams GP, Li X, et al. Peripheral monocyte entry is required for alpha-Synuclein induced inflammation and Neurodegeneration in a model of Parkinson disease. Exp Neurol. 2018;300:179-87.
42. Schonhoff AM, Figge DA, Williams GP, Jurkuvenaite A, Gallups NJ, Childers GM, et al. Border-associated macrophages mediate the neuroinflammatory response in an alpha-synuclein model of Parkinson disease. Nat Commun. 2023;14(1):3754.
43. George S, Tyson T, Rey NL, Sheridan R, Peelaerts W, Becker K, et al. T Cells Limit Accumulation of Aggregate Pathology Following Intrastriatal Injection of alpha-Synuclein Fibrils. J Parkinsons Dis. 2021;11(2):585-603.
44. Bouaboula M, Rinaldi M, Carayon P, Carillon C, Delpech B, Shire D, et al. Cannabinoid-receptor expression in human leukocytes. Eur J Biochem. 1993;214(1):173-80.

45. Castaneda JT, Harui A, Kiertscher SM, Roth JD, Roth MD. Differential expression of intracellular and extracellular CB(2) cannabinoid receptor protein by human peripheral blood leukocytes. J Neuroimmune Pharmacol. 2013;8(1):323-32.
46. Simard M, Rakotoarivelo V, Di Marzo V, Flamand N. Expression and Functions of the CB(2) Receptor in Human Leukocytes. Front Pharmacol. 2022;13:826400.
47. Liu Z, Yang N, Dong J, Tian W, Chang L, Ma J, et al. Deficiency in endocannabinoid synthase DAGLB contributes to early onset Parkinsonism and murine nigral dopaminergic neuron dysfunction. Nat Commun. 2022;13(1):3490.

Table 1. List of rat primers

Gene	Forward Sequence	Reverse Sequence
CD206	GGT TCC GGT TTG TGG AGC AG	TCC GTT TGC ATT GCC CAG TA
YM1	TGC CAA CAT CAG CAA CAA CA	CCA TCC TCC AAC AGA CAG CA
TGFb	CAC CCG CGT GCT AAT GGT	TGT GTG ATG TCT TTG GTT TTG TCA
CD80	TGC TGG TTG GTC TTT TCC A	TGA CTG CTC TTC AGA ACA AAA
TNF	TGT ACC TTA TCT ACT CCC AGG TTC TCT	GTG TGG GTG AGG AGC ACG TA
CB2	TGA CCG CTG TTG ACC GAT AC	CGA GAG GAC CCA CAT GAC AC

Table 2. Pharmacokinetic results of SMM-189 peripheral administration to mice

Matrix	Route	Dose (mg/kg)	Tmax (hr)	Cmax (ng/mL)	Brain/Plasma Ratio (Cmax)
Plasma	i.p.	6	0.50	277.07	
	p.o.	6	0.25	43.15	
Brain	i.p.	6	0.50	204.64	0.74
	p.o.	6	0.25	70.34	1.63

Figure Legends:

Figure 1. Experimental design. Rats were injected unilaterally with AAV2/5-human wild-type alpha-synuclein (cohort 1 and 2: 2.9 – 4.3E11 vg/mL) using stereotaxic coordinates to target the substantia nigra and one week later were dosed daily with peripheral injections of SMM-189, a novel CB2 inverse agonist (6mg/kg, ip) or vehicle for 7 remaining weeks until perfusion. Blood was collected at baseline and every 2-4 weeks to measure plasma drug levels. Endpoint PBMCs and brain were evaluated for changes in inflammatory pathway gene expression using qPCR and the midbrain was further used for immunohistochemistry to evaluate synuclein pathology and immune cells. An additional cohort of rats followed similar experimental design (high-titer cohort: 4.6E12 vg/mL) to evaluate immune cells in blood (PBMCs) and brain. Blood was collected at baseline, 4 weeks and 8 weeks and brains collected at either 4 or 8 weeks for flow cytometry.

Figure 2. SMM-189 decreases accumulation of pSer129 alpha-synuclein in the lesioned nigra. Representative images of pSer129 Asyn (A), proteinase K-insoluble Asyn (C), and total human Asyn (E) in rats receiving AAV2/5-hAsyn and treated with either vehicle or SMM-189. Quantification of cohort 1 and 2 rats treated with SMM-189 normalized to vehicle showed reduced pSer129 Asyn (abcam ab512253, B) compared to vehicle (p=0.0023) and a trend to reduced intensity of proteinase K-insoluble Asyn (p=0.0824, D). Total human Asyn did not differ between groups when evaluating the optical density of Asyn-ir within the lesioned nigra (F). Striatal lysates from hemispheres ipsilateral to the AAV2/5-hAsyn injections were analyzed by western blot and demonstrated that human Asyn was not different between treatments. Results suggest that peripheral CB2 modulation attenuated the aggregation of nigral h-Asyn.

Figure 3. SMM-189 modifies central neuroinflammation. Representative microphotographs of midline midbrain sections immunostained for IBA1 (A) CD68 (C). Arrows highlight the CD68+ cells included in the quantification. Quantification of IBA1+ immunofluorescent staining reveals significant lesion effect based on count and area for each treatment group (B). Two-way ANOVA with Sidak's multiple comparisons test, counts: *p=0.0115, **p=0.0028, area: *p=0.0129, **p=0.0005. CD68 quantification using ImageJ particle counting and normalized to vehicle found significant increases in SMM-189 compared to vehicle-treated rats, while CD163 quantification within the lesioned nigra was decreased by SMM-189 treatment (D). The mRNA expression of inflammatory cytokines CD206, YM1, TGFβ, CD80, TNF, CB2 are displayed for both frontal cortex (E) and PBMCs (F). Relative PBMC mRNA abundance was normalized to GAPDH, frontal cortex to HPRT1. Unpaired t test, Frontal cortex: YM1, *p=0.0291. CD206, *p=0.0107. PBMC: *p=0.0204, **p=0.0084.

Figure 4. SMM-189 globally reduces infiltrating monocytes and brain cell activation at 4 weeks. Brain immune cells were isolated from lesioned (+human Asyn) and non-lesioned (-human Asyn) rat hemispheres at 4 weeks and monocyte, lymphocyte and microglia populations (A-C) initially identified from CD45 and CD11b expression and further gated into more distinct populations. Quantification of immune cell population frequencies are shown here for microglia (CD45loCD11b+), monocytes (CD11b+CD172a+) and lymphocytes (CD3+) of their parent gate (A-C). Monocyte frequencies are reduced in SMM-189 rats in the unlesioned hemisphere (B). Two-way ANOVA with uncorrected Fisher's multiple comparisons test, *p=0.0308. No differences were seen in quantification of non-classical (CD43+CD172a+) or classical (CD43-

CD172+) monocytes or macrophages (CD163+CD43-) frequencies (D-F). MHCII+ activated classical monocytes were no different between treatment (G). Mean fluorescent intensity (MFI) of CD172 was reduced in unlesioned hemispheres of those with SMM-189- treatment compared to vehicle treatment (H). Two-way ANOVA with uncorrected Fisher's multiple comparisons test, **p=0.0079. Mean fluorescent intensity (MFI) of CD11b was reduced in unlesioned hemispheres of those with SMM-189 treatment compared to vehicle (*p=0.0241) and also found significantly lower than SMM-189 lesioned hemispheres (I), suggesting a lesion effect (*p=0.016). CD4 and CD8 T cell subsets were quantified and found that CD4+ T cells were reduced in lesioned hemispheres of SMM-189 rats compared to vehicle (*p=0.0109), resulting in reduced CD4:CD8 ratios in across same groups (*p=0.0406; J-L).

Figure 5. Infiltrating monocytes are maintained from SMM-189, resulting in increased immune activation and CD4 at 8 weeks. Brain immune cells were isolated from lesioned-(+human Asyn) and non-lesioned (-human Asyn) hemispheres at 8 weeks and monocyte, lymphocyte and microglia populations (A-C) initially identified using CD45 and CD11b expression and further gated into more distinct populations. Quantification of immune cell population frequencies are shown here for microglia (CD45loCD11b+), monocytes (CD11b+CD172a+) and lymphocytes (CD3+) of their parent gate (A-C). Monocyte frequencies were decreased in the vehicle treated lesioned hemisphere compared to its unlesioned counterpart, but was increased in SMM-189 rats in the unlesioned hemisphere (B). Two-way ANOVA with uncorrected Fisher's multiple comparisons test, *p=0.0106, **p=0.0071. Lymphocytes frequencies were decreased in unlesioned hemisphere of those with SMM-189 treatment compared to vehicle. Two-way ANOVA with uncorrected Fisher's multiple comparisons test, *p=0.0332. No differences were seen in quantification of non-classical (CD43+CD172a+) or classical (CD43-CD172+) monocytes (D,E). Yet significant reductions were found in macrophage (CD163+CD43-) frequencies (p=0.0146) and increases in MHCII+ activated classical monocytes (p=0.0213) in lesioned hemispheres from SMM-189 treatment compared to control (F-G). Mean fluorescent intensity (MFI) of CD172 was not different between conditions (H), but mean fluorescent intensity (MFI) of CD11b was increased in unlesioned hemispheres of those with SMM-189 treatment compared to vehicle (*p=0.0162, I). CD4 and CD8 T cell subsets were quantified and found that CD4+ T cells were increased (lesion: p=0.0115; unlesion: p=0.0152), while CD8+ T cells were reduced (lesion: p=0.0064; unlesion: p=0.0056) in both hemispheres of SMM-189-treated rats compared to vehicle, resulting in increased CD4:CD8 ratios across treatment groups (lesion: p=0.0018; unlesion: p=0.0055; J-L).

Figure 6. **SMM-189 skews PBMC phenotype toward increases in circulating wound healing non-classical monocytes.** Peripheral blood mononuclear cells were isolated from whole blood at baseline, 4 and 8 weeks after AAV2/5-hAsyn injections from rats in the high-titer cohort. SMM-189 treatment resulted in increased circulating CD43+ non-classical monocytes (CD11b+CD172a+) at 8 weeks compared to vehicle treatment (p=0.0493; A), and no change in His48+ non-classical monocytes (C). SMM-189 treatment did not significantly alter the frequency of CD43- classical monocytes (CD11b+CD172a+) at any timepoint (B), but decreased specific subset of His48+ activated CD43- classical monocytes at 8 weeks compared to vehicle (p=0.0316; D). Frequency of granulocytes as defined by CD3- and granularity (SSC) were decreased at 8 weeks from SMM-189 treatment compared to vehicle (p=0.0193, E).

Figure 7. SMM-189 increases RAW264.7 macrophage phagocytosis after an inflammagen challenge. RAW264.7 macrophage cultures were challenged with either 100ng/mL (A) or 1000 ng/mL (B) lipopolysaccharide and pre-treated with SMM-189 and 24 hours later incubated with pHrodo E. coli. Treatments are analyzed across time using a one-way ANOVA with Dunnett's multiple comparisons test. Data are representative of 2 separate experiments. Representative GFP images of fluorescent pH rodo E. coli at 12 hours after the start of the phagocytosis assay for LPS + vehicle (C), LPS + 3uM SMM-189 (D), LPS + 7uM SMM-189 (E) conditions.

Supplemental Figures

Table S1. Myeloid PBMC flow panel

Antibody	Manufacturer	Product number	Dilution
anti-Rat CD45-BUV395	BD Biosciences	740258	1:50
anti-Rat His48-FITC	Invitrogen	11-0570-82	1:200
Anti-Rat CD43-PE-Vio770	Miltenyi	130-107-721	1:100
Anti-rat CD3-Viogreen	Miltenyi	130-103-126	1:200
Anti-rat CD4-APC-Vio770	Miltenyi	130-107-504	1:100
Anti-ms/rat MHCII-PerCP-Vio700	Miltenyi	130-107-877	1:100
Anti-rat CD11b-Pac Blue	BioRad	MCA275PB	1:50
Anti-rat RP1-BV786	BD Biosciences	743058	1:20
Anti-rat CD172a-APC	R&D systems	FAB7307A	1:100
Anti-rat CD32	BD Biosciences	550271	1:100

Table S2. Lymphoid PBMC flow panel

Antibody	Manufacturer	Product number	Dilution
Anti-rat CD45RA-PECy7	Biolegend	202315	1:200
Anti-rat CD3-Viogreen	Miltenyi	130-103-126	1:200
Anti-rat CD4-APC-Vio770	Miltenyi	130-107-504	1:100
Anti-CD8a-PerCP-Vio700	Miltenyi	130-108-914	1:100
Anti-rat CD25-BV786	BD Biosciences	742757	1:50
Anti-ms/rat Foxp3-AF647 *stained following intracellular permeabilization	R&D systems	FAB7307A	1:50

Anti-rat CD32	BD Biosciences	550271	1:100

Table S3. Brain Immune cell flow panel

Antibody	Manufacturer	Product number	Dilution
anti-Rat CD44H-FITC	Miltenyi	130-107-854	1:50
Anti-Rat CD62L-PE	BD Biosciences	551398	1:200
Anti-rat CD45RA-PECy7	Biolegend	202315	1:200
Anti-rat CD3-Viogreen	Miltenyi	130-103-126	1:200
Anti-rat CD4-APC-Vio770	Miltenyi	130-107-504	1:100
Anti-CD8a-PerCP-Vio700	Miltenyi	130-108-914	1:100
Anti-rat CD25-BV786	BD Biosciences	742757	1:50
Anti-ms/rat Foxp3-AF647 *stained following intracellular permeabilization	R&D systems	FAB7307A	1:50
Anti-rat CD32	BD Biosciences	550271	1:100

Table S4. Western and IHC antibodies

Antibody	**Company**	**Product #**	**Loading protein concentration**	**Concentration**
Western antibodies				
TH	Millipore	AB152	10ug	1:2000
Asyn (4B12)	BioLegend	807801	10ug	1:500
DAT	Novus Bio	NBP2-22164	10ug	1:2000
IBA1	Abcam	AB5076	10ug	1:1500
Phospho-TH	Phospho solutions	P1580-40	10ug	1:1000
NFκB p65	Santa Cruz	SC327	15ug	1:500
GFAP	Dako	Z0334	15ug	1:2500
pSer129 (EP1536Y)	Abcam	AB51253	15ug	1:500
IHC antibodies				
IBA1	Wako	019-19741		1:500
TH	Immunostar	22941		1:1000
Asyn (4B12)	BioLegend	807801		1:2500
pSer129 (EP1536Y)	Abcam	AB51253		1:2500
CD68	Sertec	MCA341R		1:2000
MHCII	Biorad	MCA46GA		1:1000

CD163	Biorad	MCA342R		1:1000

Figure S1. Gating strategy for rat brain immune cells. *Cells were initially* by SSC and FSC, doublets excluded and live cells selected as those that did not take up live/dead fixable stain. Live cells were further gated by CD45 and CD11b where microglia (CD45lo, CD11b+), lymphocyte (CD45+CD11b-), and monocytes (CD45hi, CD11b+) populations were identified. Microglia subsets were further defined by the presence of either MHCII or CD172a frequencies and MFI. Monocytes were gated on CD3-, and further defined by CD11b+/CD172a+. Two populations of monocytes were identified CD43lo (classical monocytes) and CD43hi (non-classical monocytes) and monocyte activation determined by frequencies and MFI of MHCII, CD172a, and CD163 (macrophage marker). Lymphocytes were gated as CD3+ and further defined by CD4 and CD8 expression.

Figure S2. Gating strategy for rat monocytes. Cells were initially identified by SSC and FSC, doublets excluded and live cells selected as those that did not take up live/dead fixable stain. Monocytes were gated on CD3-, granulocytes excluded by size with high SSC, and further defined by CD11b+/CD172a+. Two populations of monocytes were identified CD43lo/HIS48+ (classical monocytes) and CD43hi/His48lo (non-classical monocytes) and monocyte activation determined by MHCII MFI.

Figure S3. Gating strategy for rat lymphocytes and elevated peripheral Tregs in SMM-189-treated rats after 7 weeks of dosing. Cells were initially identified by SSC and FSC, doublets excluded and live cells selected as those that did not take up live/dead fixable stain. Lymphocytes were gated as CD3+ and subpopulations of CD4+ defined as Tregs (foxp3+) with subpopulations separated by CD25 expression. B cells were identified as CD3-CD45RA+ populations. PBMCs were evaluated by flow cytometry at baseline, 4 and 8 weeks after AAV2/5-hAsyn. No differences in T cell CD4+ or CD8+ populations were seen between treatments at any timepoints. However, there was a significant increase of CD4+ Tregs (Foxp3+ and Foxp3+/CD25+) found between baseline and 8 weeks after AAV2/5-hAsyn in SMM-189 treated rats.

Figure S4. Targeting of rAAV2/5-hwtAsyn in the rat substantia nigra. Representative immunofluorescent staining of tyrosine hydroxylase (TH; red) and Asyn (green) with DAPI (blue) demonstrating unilateral presence of Asyn in the TH+ nigra neurons. Scale bar 300μm.

Figure S5. Animal body weights and SMM-189 plasma and CSF levels. Weekly body weights did not demonstrate differences between treatment groups over 8 weeks for either cohort 1, 2 or high-titer cohort (A, C, F). Blood was collected from the tail vein at baseline and every 2 weeks post-AAV. Cohort 1 blood was collected approximately 24 hours after the previous day SMM-189 dose and found generally significant increases in SMM-189 blood concentrations overtime (B). Whereas, cohort 2 and high-titer cohorts had blood collected from tail vein approximately 2 hours after SMM-189 or vehicle dose. Significant increases were seen in the level of plasma SMM-189 in animals receiving SMM-189 treatment at both 4 and 8 weeks in SMM-189 treated rats compared to vehicle treatment (D, G). CSF was collected at endpoint and ~2 hours after peripheral treatment of either vehicle or SMM-189 in cohort 2 animals. Low levels of drug in SMM-189 treated animals may suggest low penetrance into CNS.

Figure S6. Striatum does not reveal any protein expression changes in astrocytes, microglia or dopamine markers. Representative blots for GFAP (50KDa) and IBA1 (17KDa) of striatal lysates from ipsilateral and contralateral hemispheres. Quantification of GFAP and IBA1 relative expression normalized to its own total protein and as a ratio of ipsilateral to contralateral levels show no difference between treatment groups. Striatal TH, phosphoTH and dopamine transporter (DAT) protein expression normalized to its own total protein and to the contralateral hemisphere of vehicle-treated rats show no differences between treatments with a strong trend to increased DAT in SMM-189-treated rat ipsilateral striatum.

Figure S7. Plasma and CSF cytokine levels do not change as a result of CB2 modulation. Plasma concentrations of cytokines IL-10, TNF and IL1β and CSF concentrations of cytokines IL-10, TNF and IL1β and IL-6 are not significantly different between treatment groups.

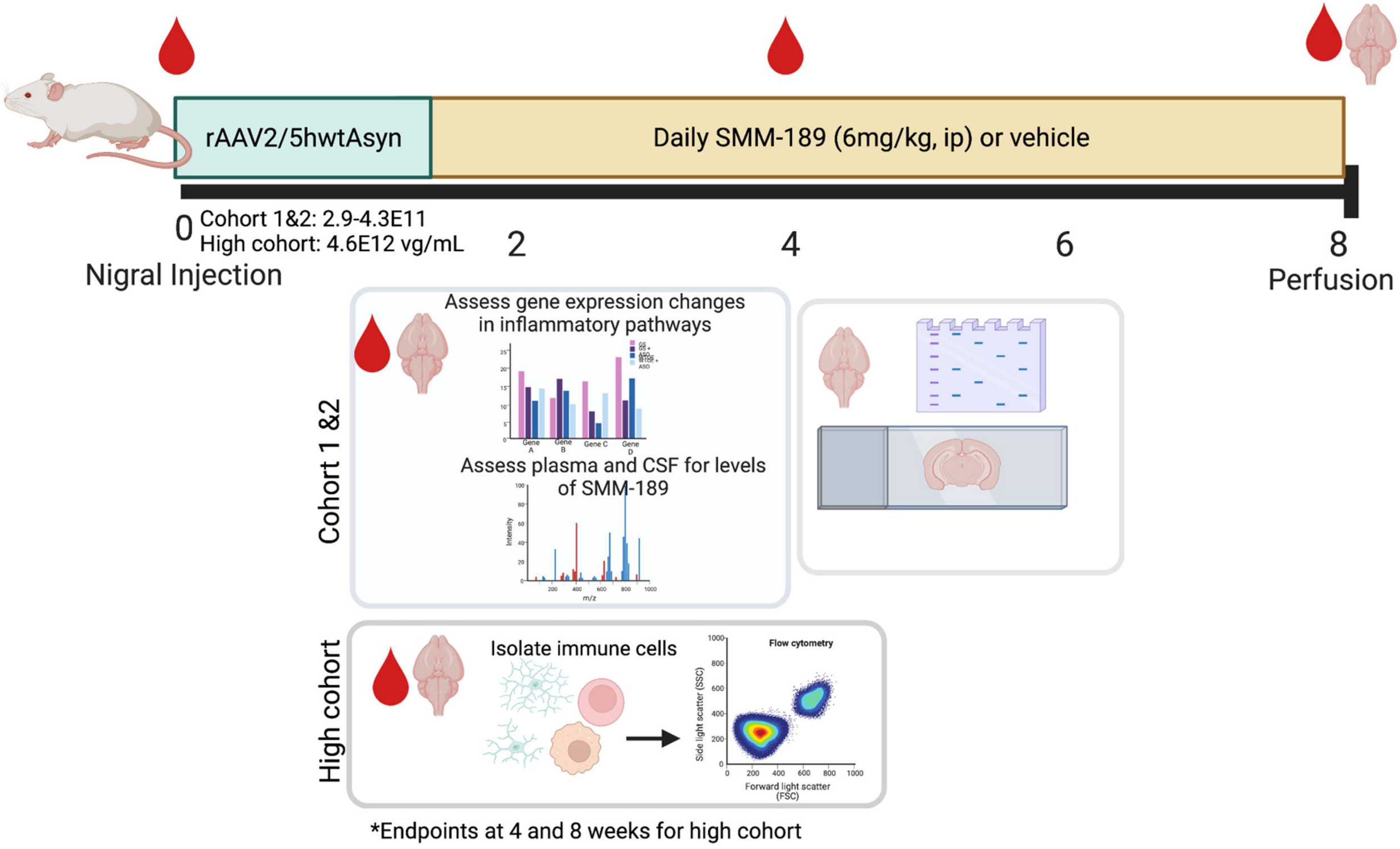

Figure 1. Experimental design

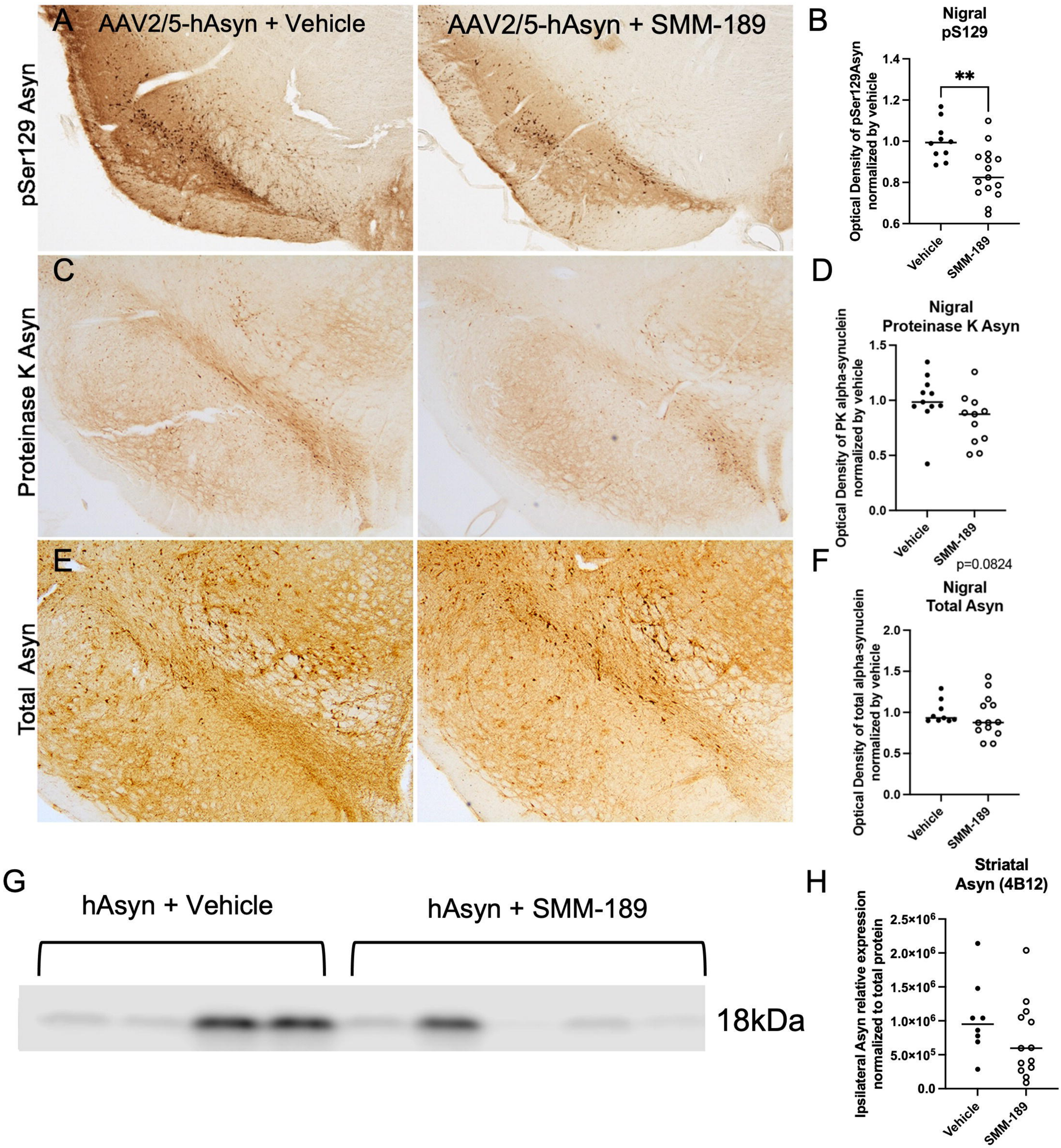

Figure 2. SMM-189 decreases accumulation of pSer129 alpha-synuclein in the lesioned nigra

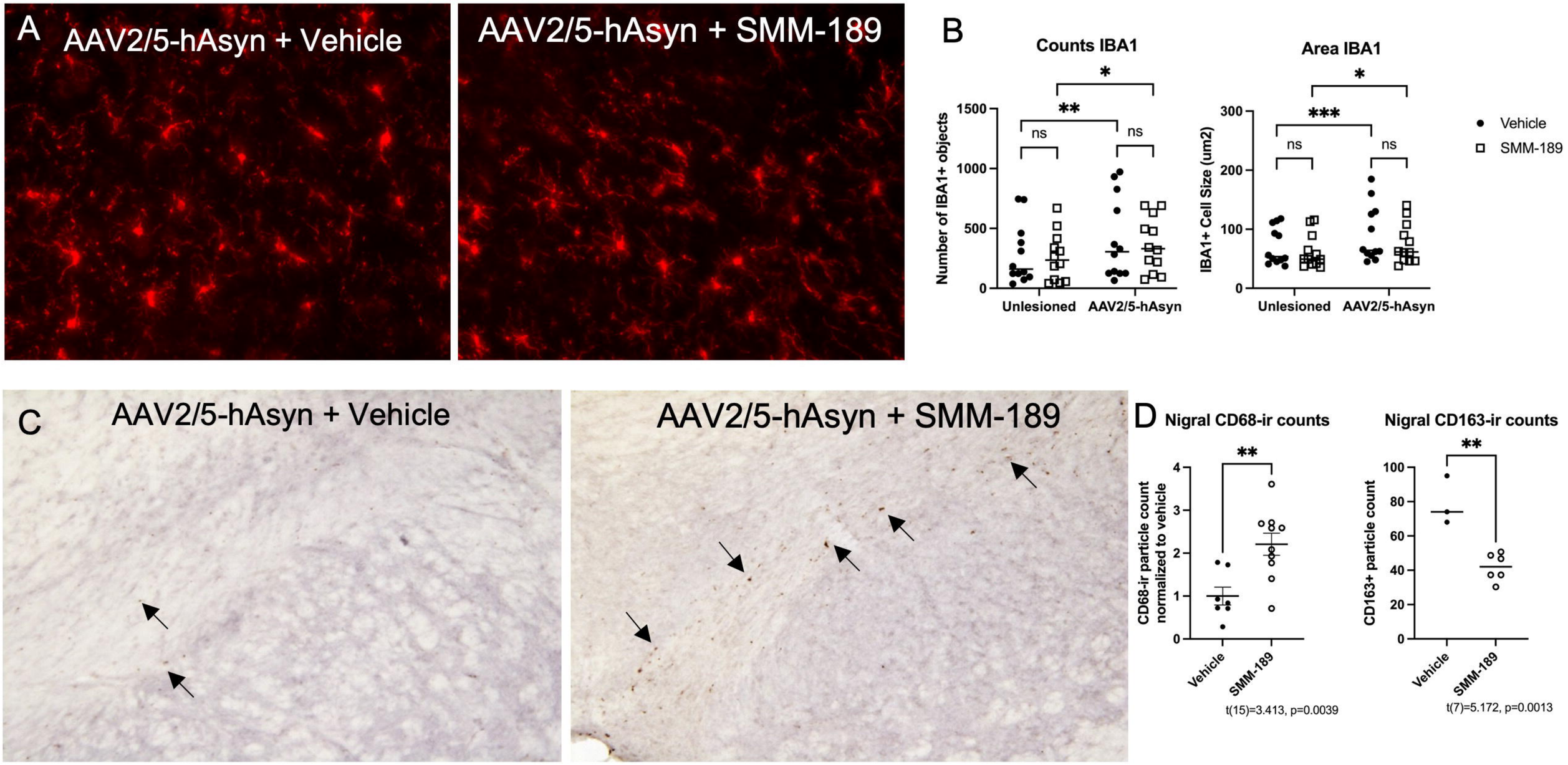

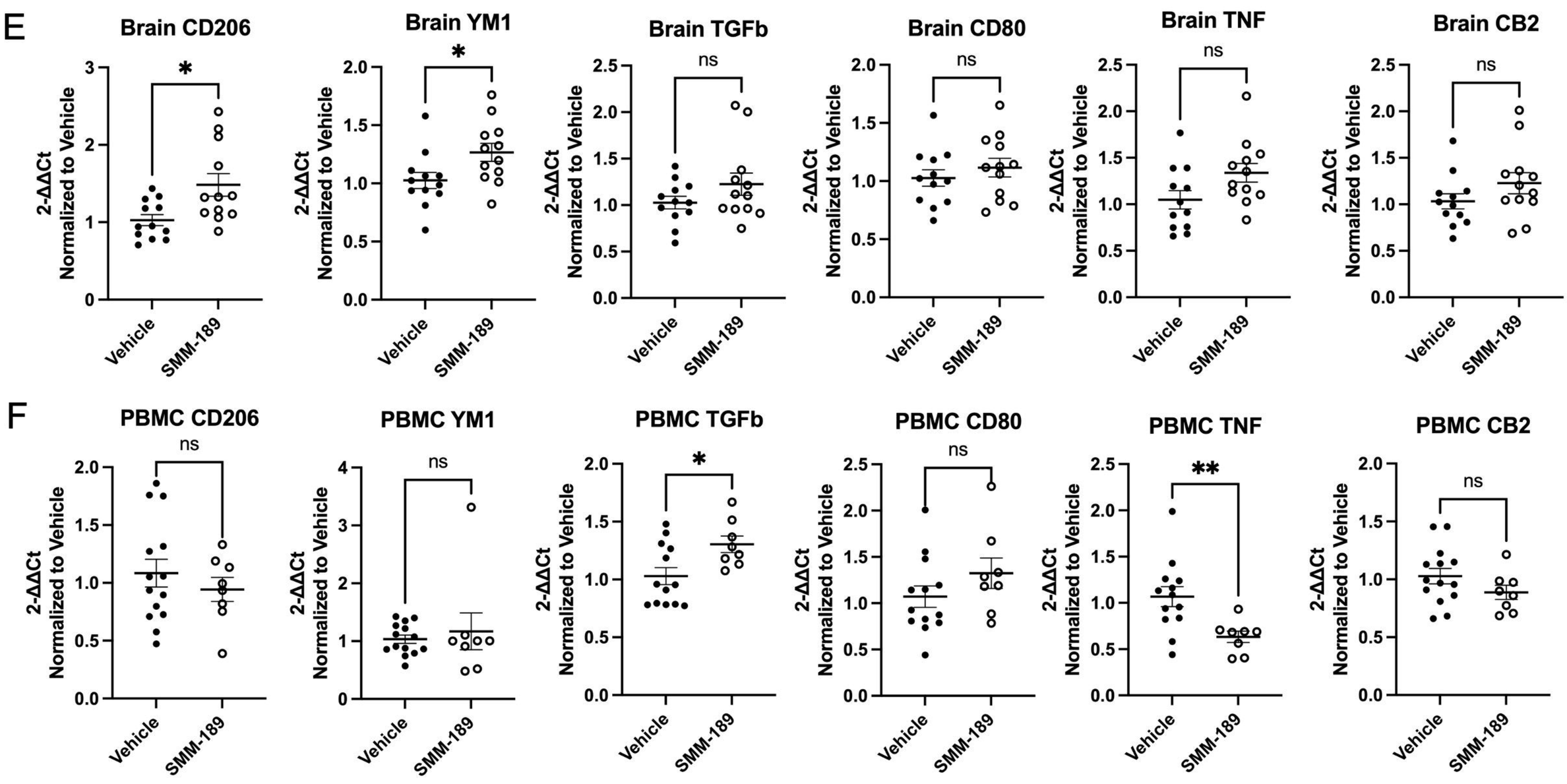

Figure 3. SMM-189 modifies central neuroinflammation

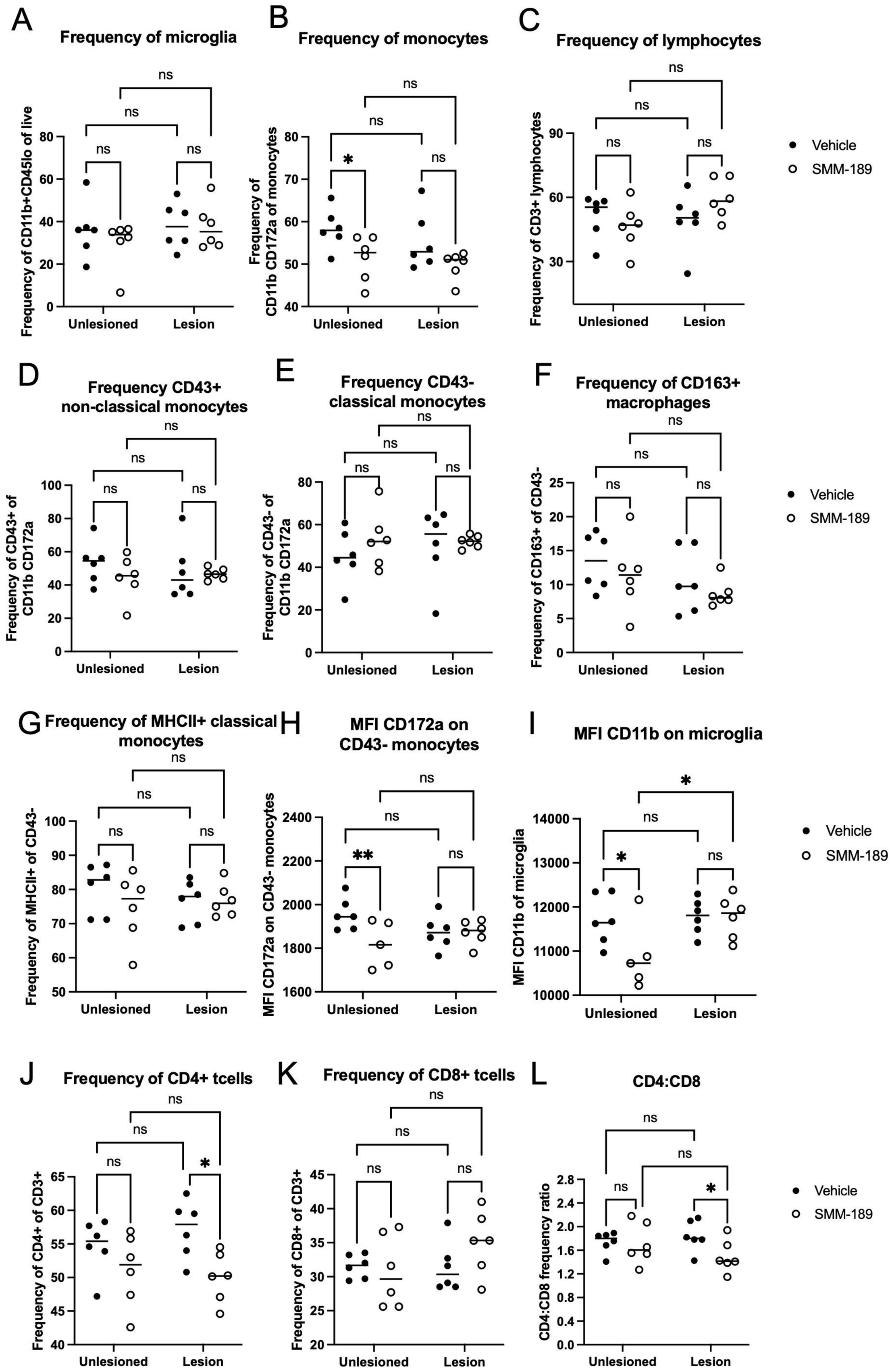

Figure 4. SMM-189 globally reduces infiltrating monocytes and brain cell activation at 4 weeks

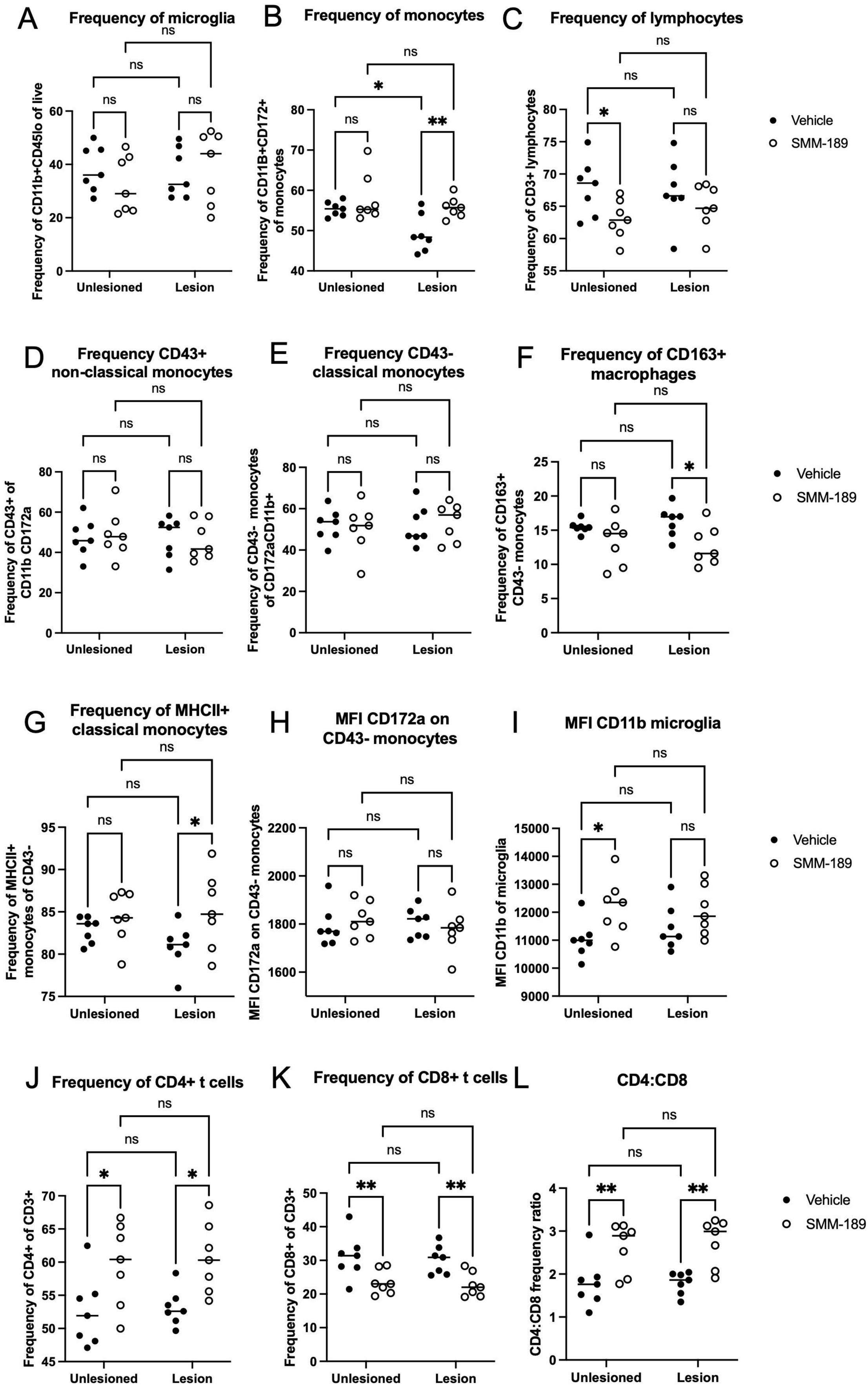

Figure 5. Infiltrating monocytes are maintained from SMM-189, resulting in increased immune activation and CD4 at 8 weeks

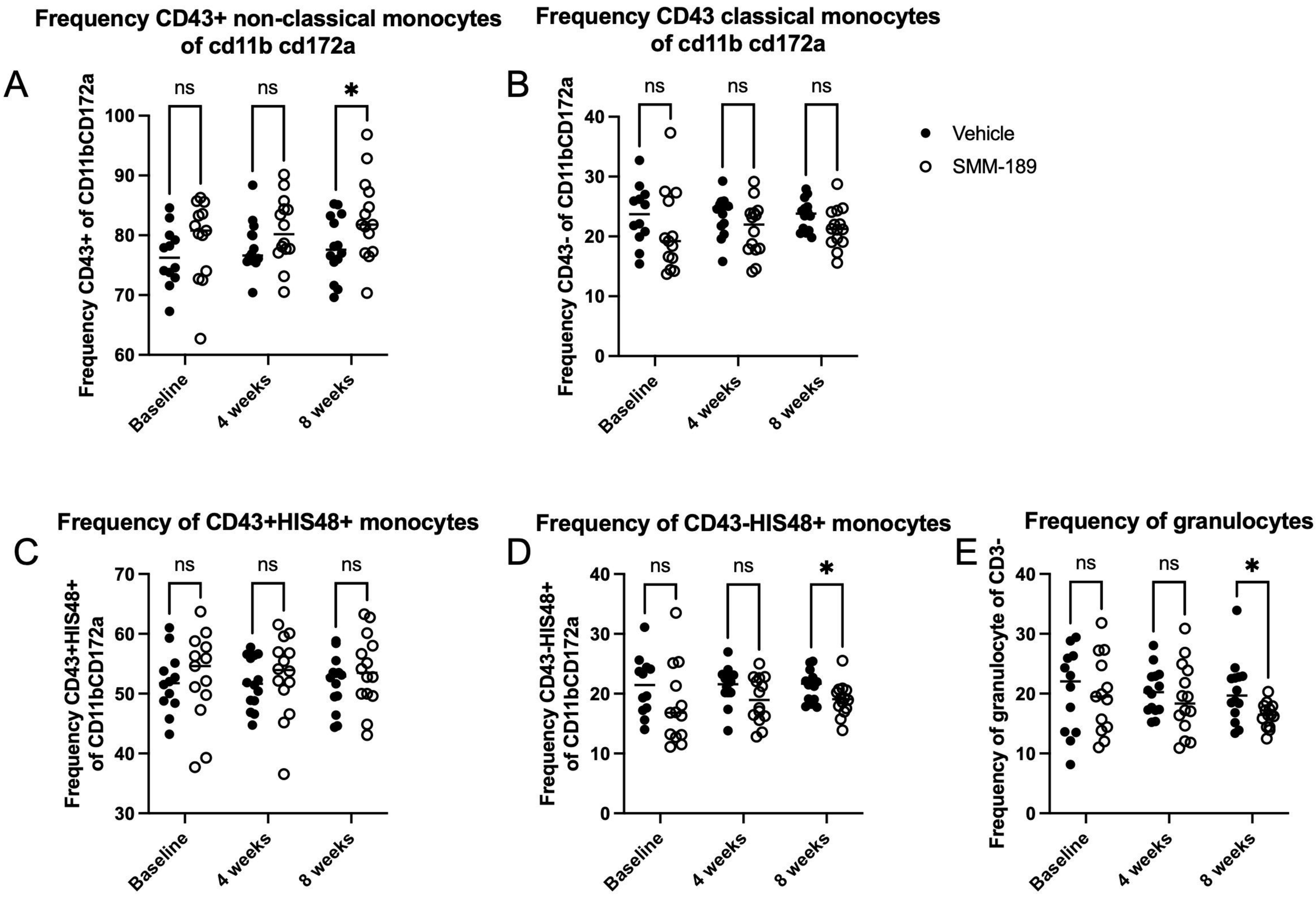

Figure 6. SMM-189 skews PBMC phenotype toward increases in circulating wound healing non-classical monocytes

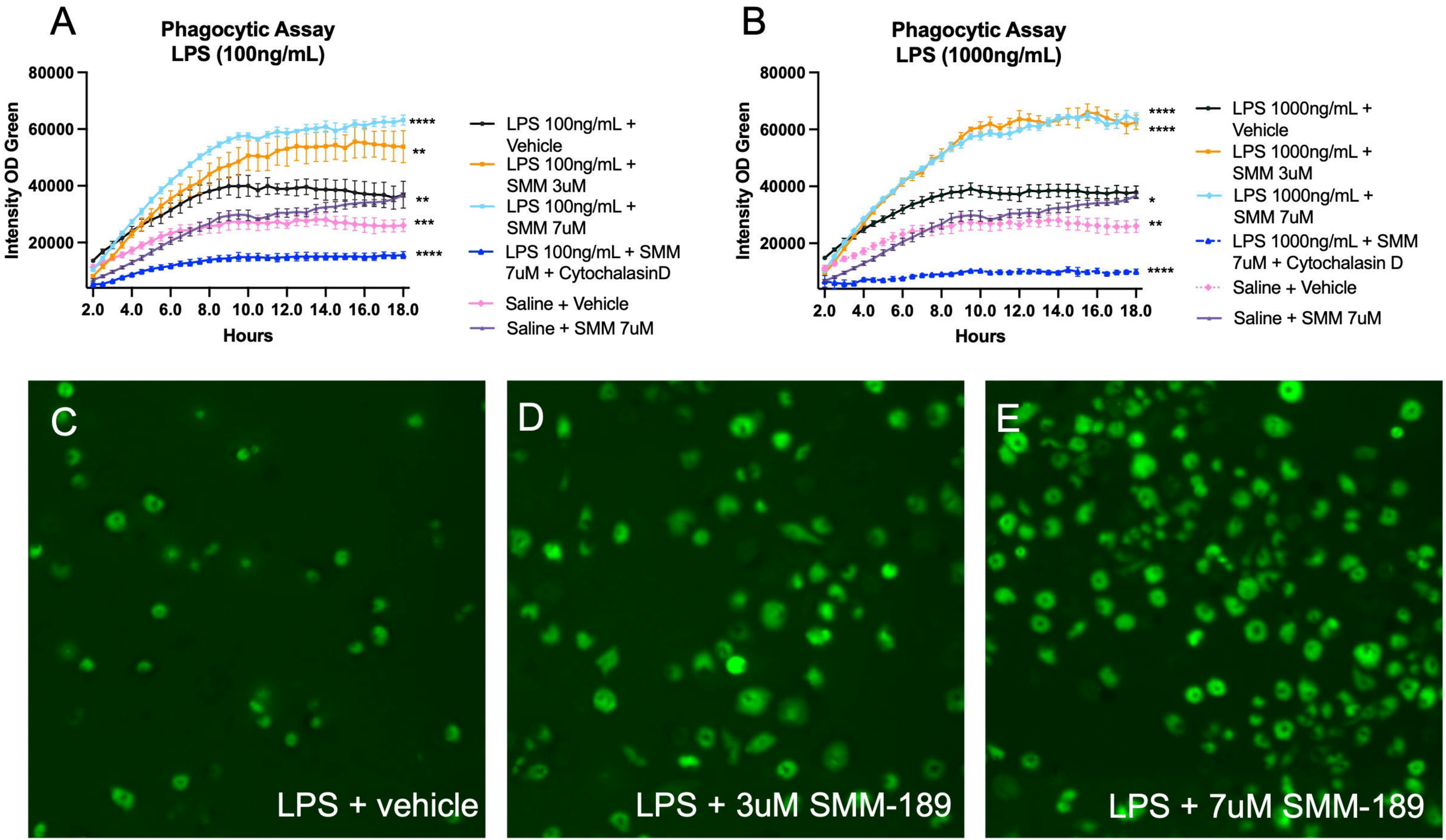

Figure 7. SMM-189 increases RAW264.7 macrophage phagocytosis after an inflammagen challenge

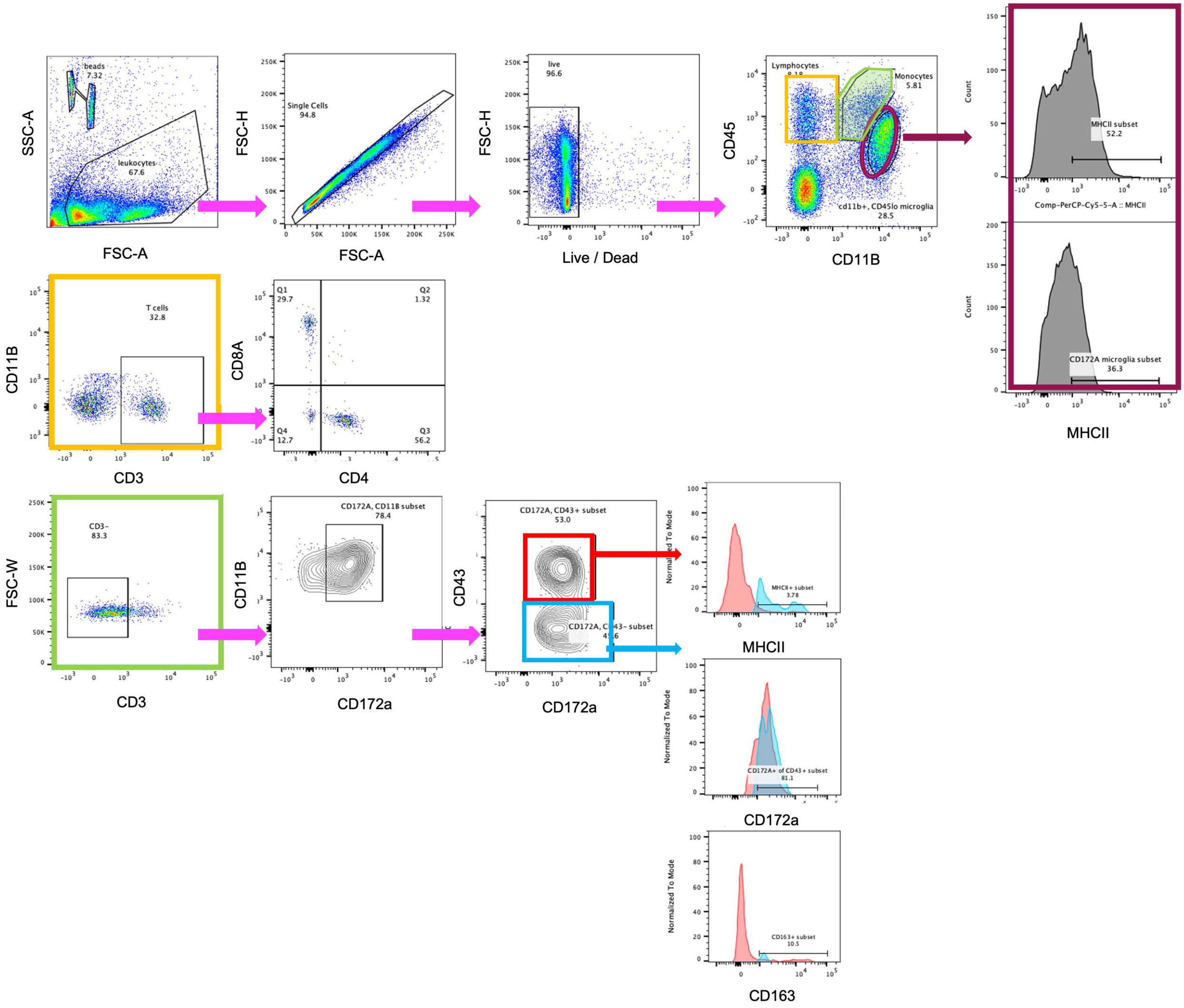

Figure S1. Gating strategy for rat brain immune cells

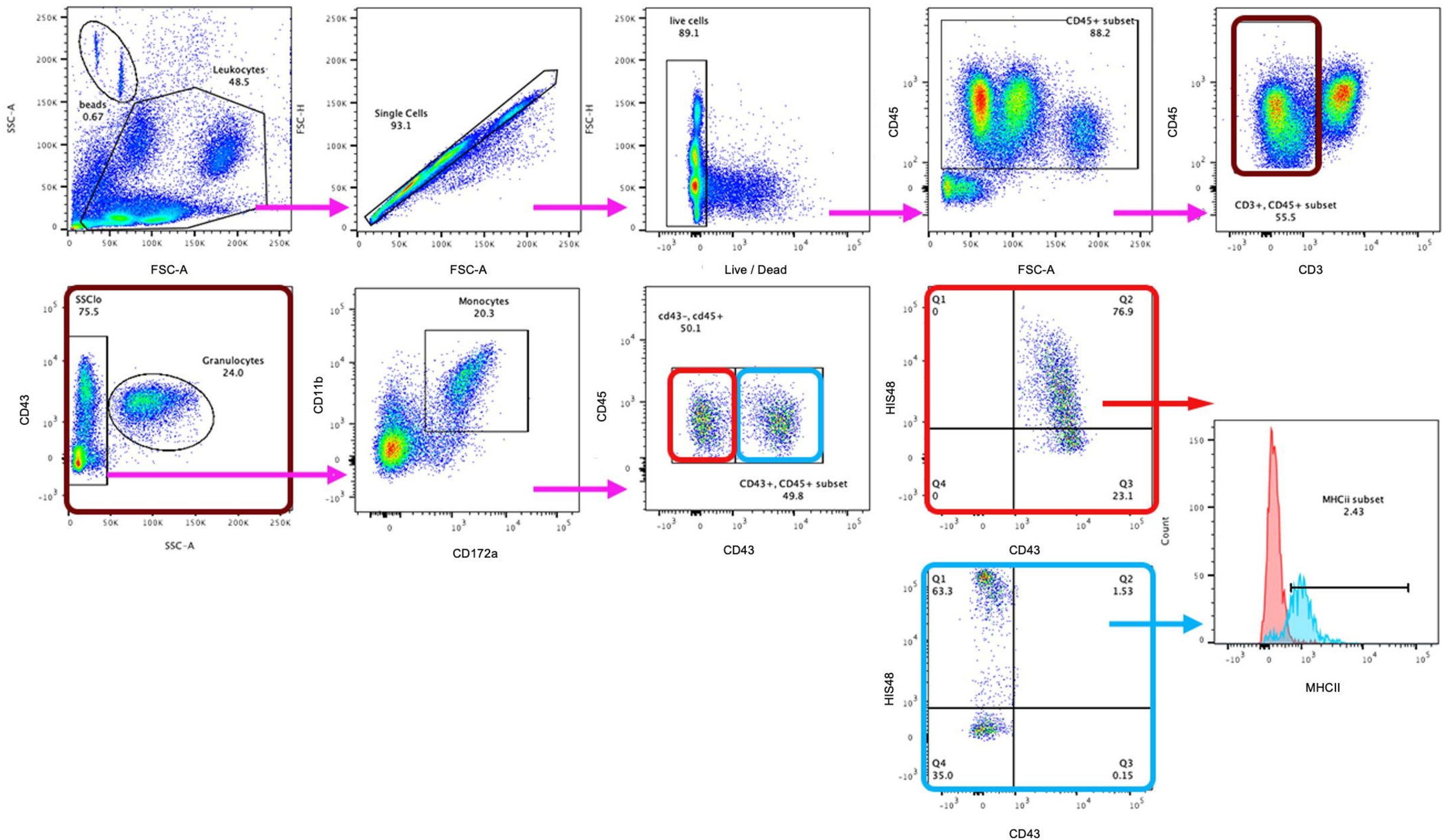

Figure S2. Gating strategy for rat monocytes

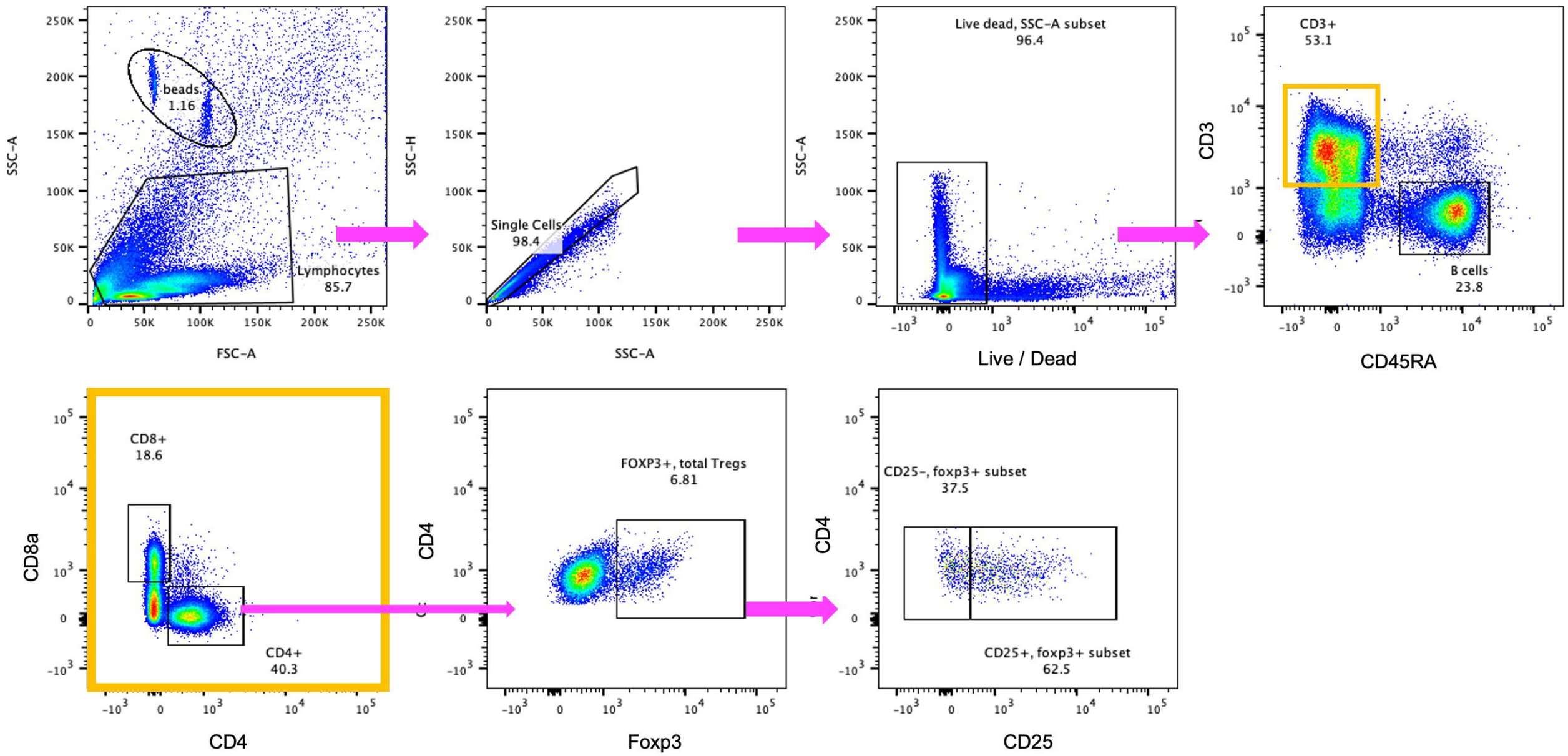

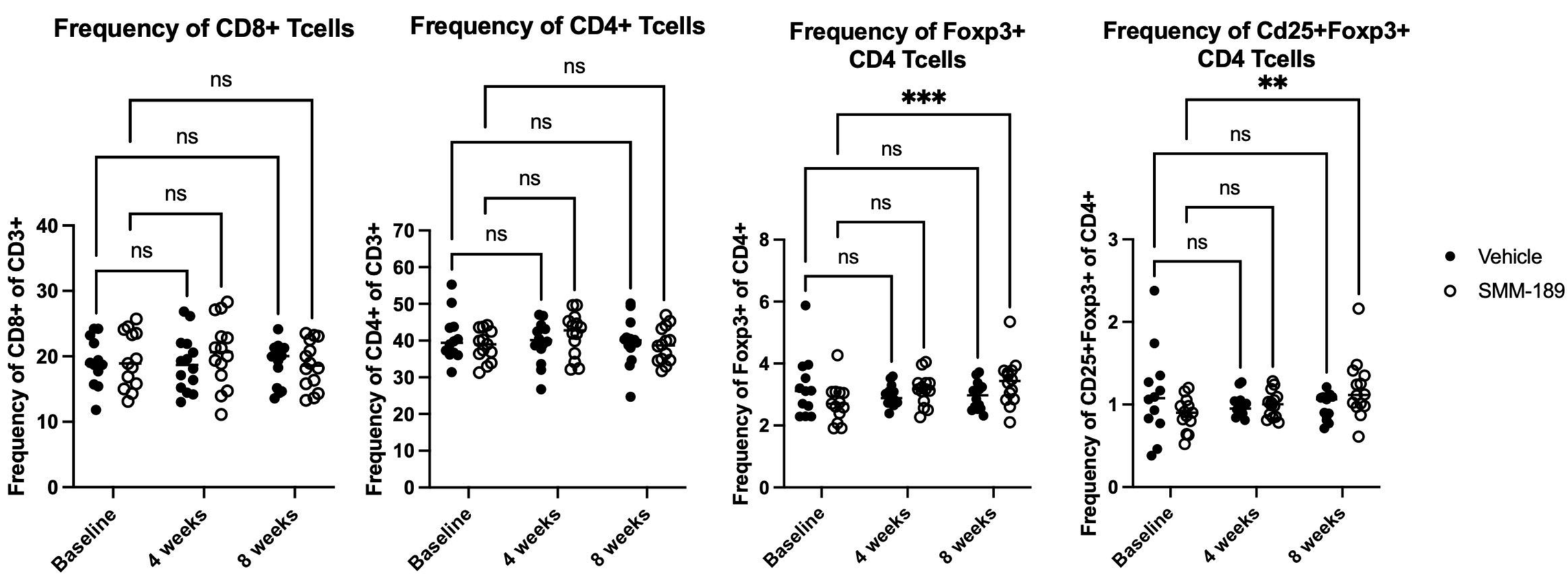

Figure S3. Gating strategy for rat lymphocytes and elevated peripheral Tregs in SMM-189-treated rats after 7 weeks of dosing

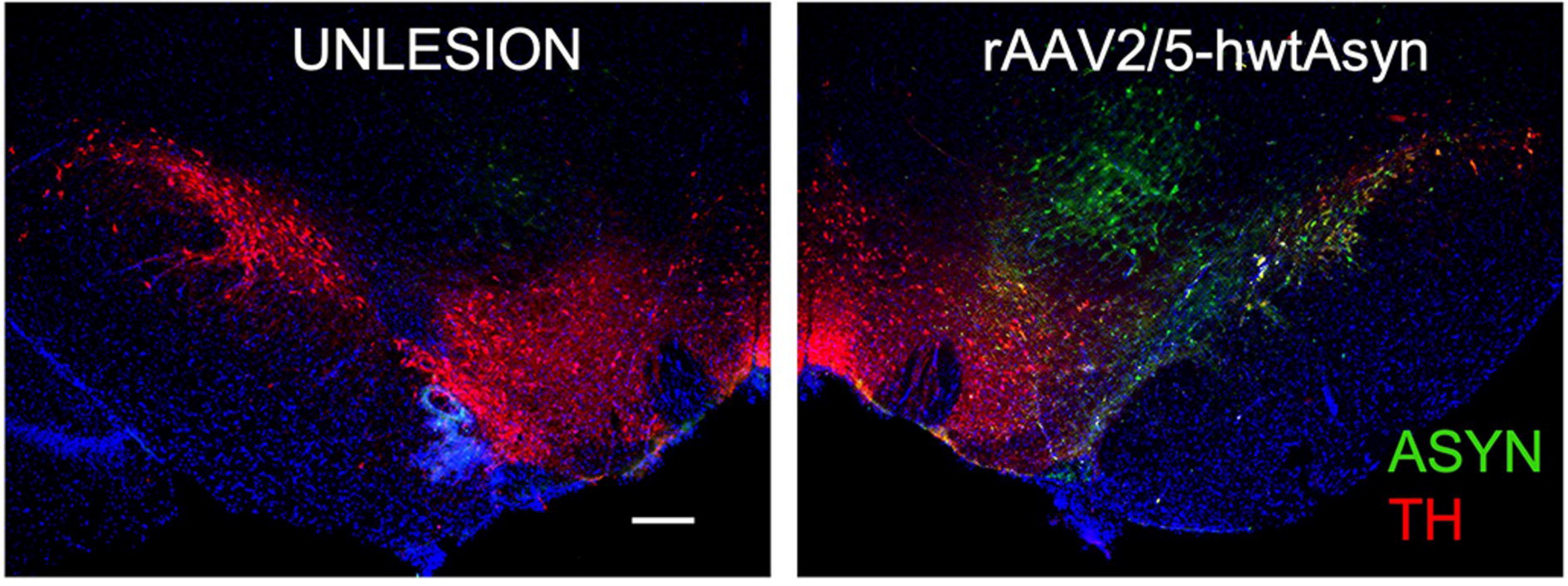

Figure S4. Targeting of rAAV2/5-hwtAsyn in the rat substantia nigra

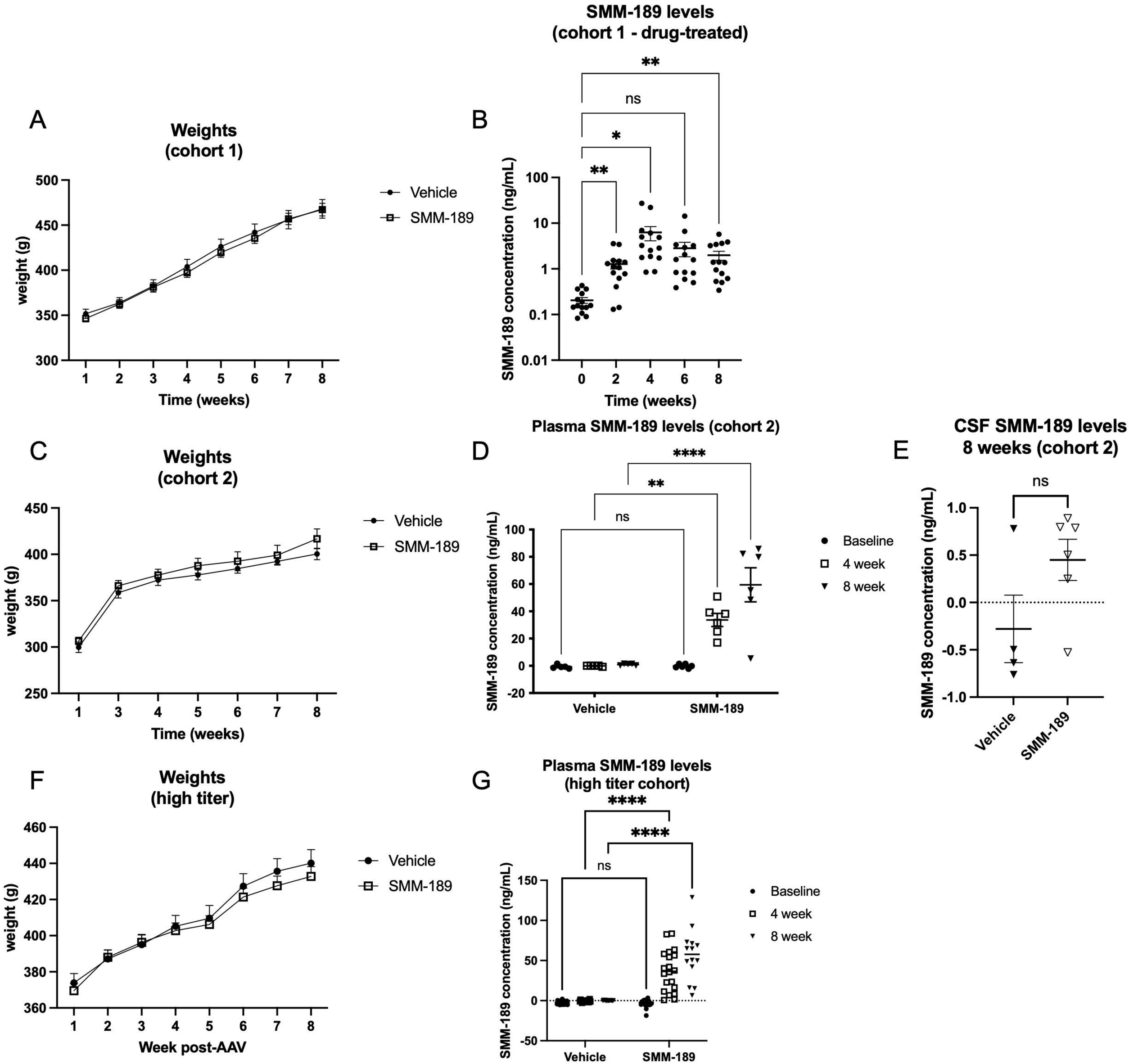

Figure S5. Animal body weights and SMM-189 plasma and CSF levels

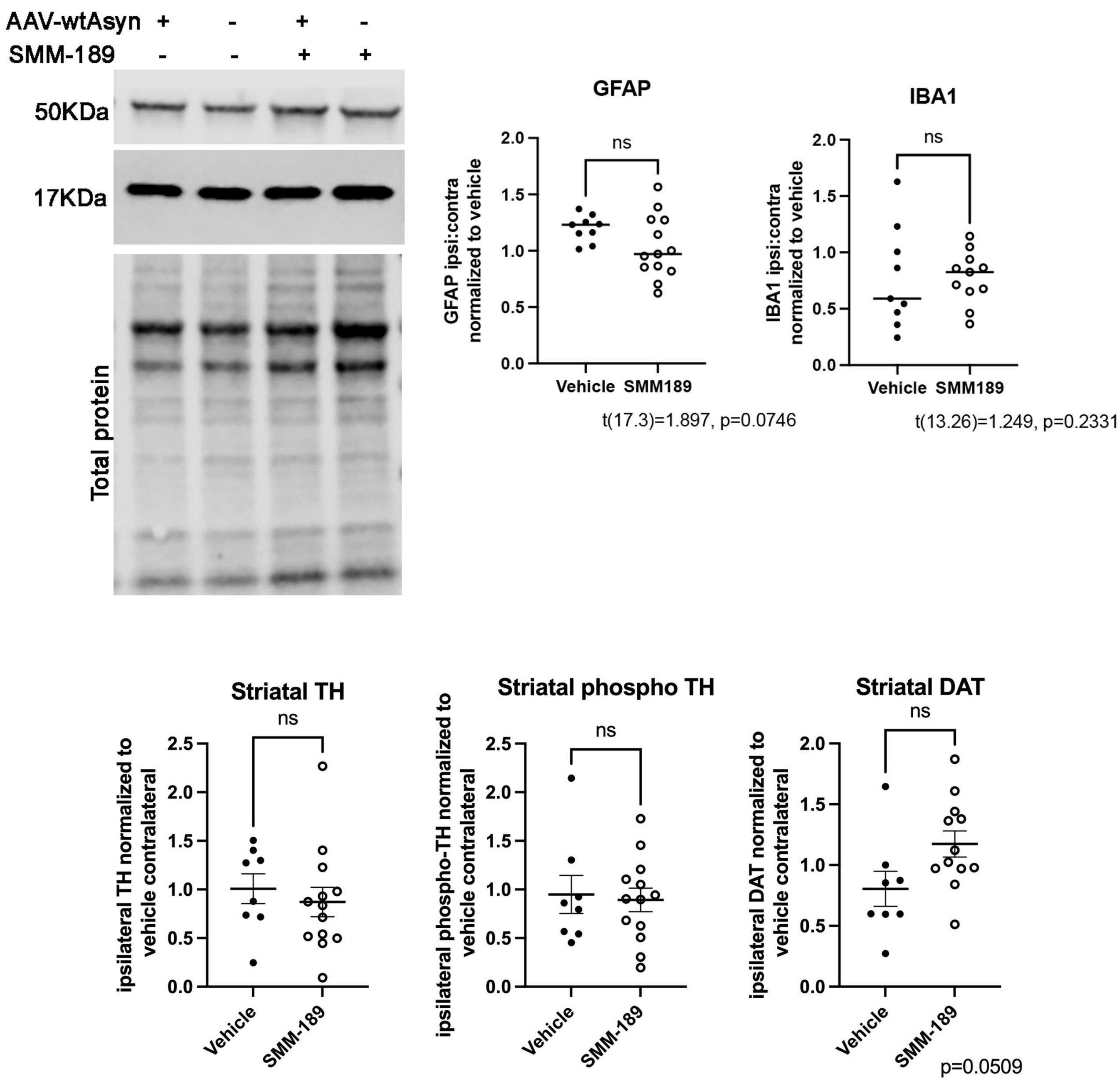

Figure S6. Striatum does not reveal any protein expression changes in astrocytes, microglia or dopamine markers

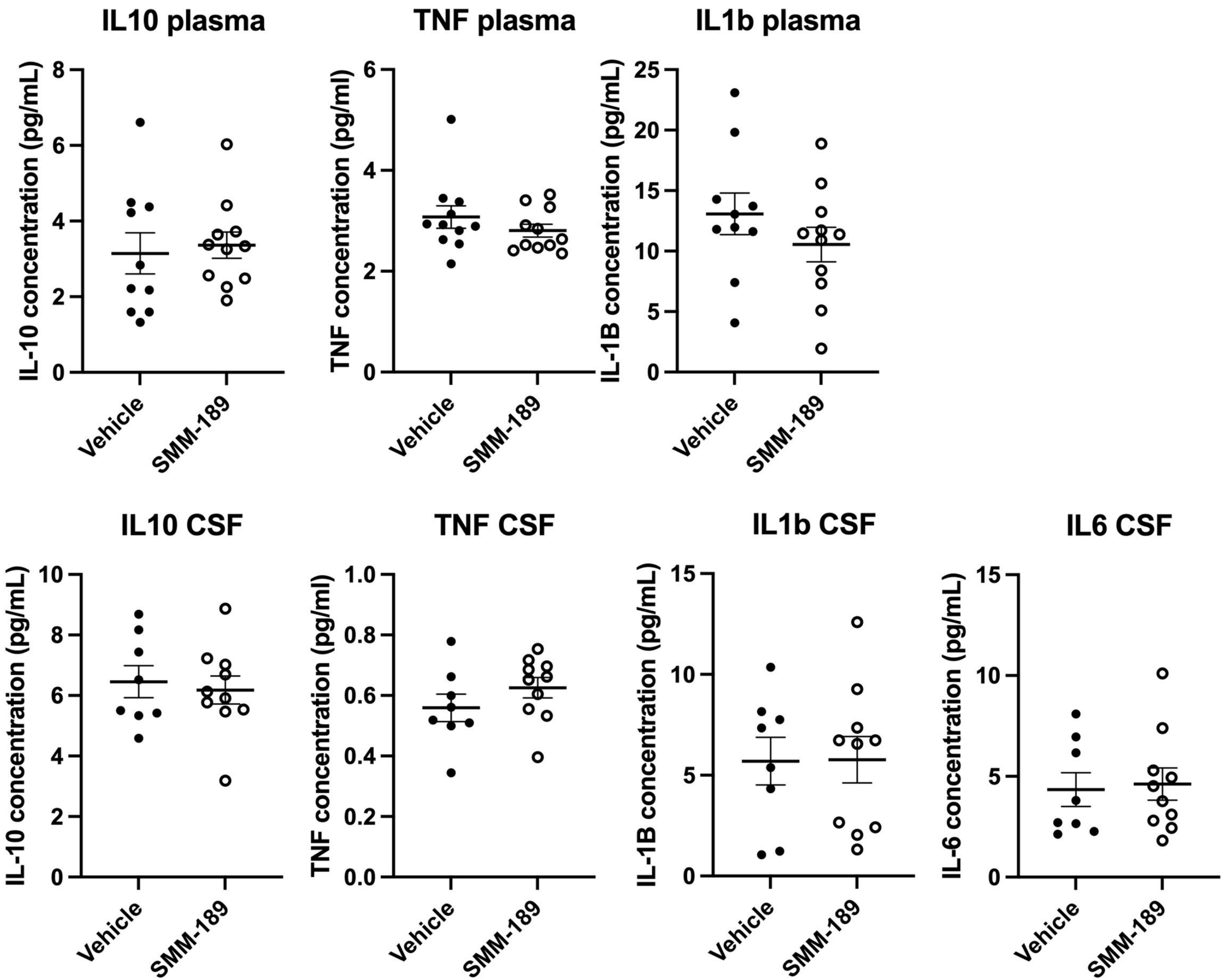

Figure S7. Plasma and CSF cytokine levels do not change as a result of CB2 modulation